© 2020. Published by The Company of Biologists Ltd | Journal of Cell Science (2020) 133, jcs245845. doi:10.1242/jcs.245845

RESEARCH ARTICLE

Mucin-type *O*-glycosylation controls pluripotency in mouse embryonic stem cells via Wnt receptor endocytosis

Federico Pecori[1], Yoshihiro Akimoto[2], Hisatoshi Hanamatsu[3], Jun-ichi Furukawa[3], Yasuro Shinohara[4], Yuzuru Ikehara[5] and Shoko Nishihara[1,6,*]

ABSTRACT

Mouse embryonic stem cells (ESCs) can differentiate into a range of cell types during development, and this pluripotency is regulated by various extrinsic and intrinsic factors. Mucin-type *O*-glycosylation has been suggested to be a potential factor in the control of ESC pluripotency, and is characterized by the addition of *N*-acetylgalactosamine (GalNAc) to serine or threonine residues of membrane-anchored proteins and secreted proteins. To date, the relationship between mucin-type *O*-glycosylation and signaling in ESCs remains undefined. Here, we identify the elongation pathway via C1GalT1 that synthesizes T antigen (Galβ1-3GalNAc) as the most prominent among mucin-type *O*-glycosylation modifications in ESCs. Moreover, we show that mucin-type *O*-glycosylation on the Wnt signaling receptor frizzled-5 (Fzd5) regulates its endocytosis via galectin-3 binding to T antigen, and that reduction of T antigen results in the exit of the ESCs from pluripotency via canonical Wnt signaling activation. Our findings reveal a novel regulatory mechanism that modulates Wnt signaling and, consequently, ESC pluripotency.

This article has an associated First Person interview with the first author of the paper.

KEY WORDS: C1GalT1, Embryonic stem cells, Glycosylation, Pluripotency, T antigen, Wnt signaling pathway

INTRODUCTION

Mouse embryonic stem cells (ESCs) are pluripotent stem cells derived from preimplantation embryos and have the capability of differentiating into cells of the three germ layers (Evans and Kaufman, 1981). A large number of studies have explored the potential applications of ESCs for research into developmental biology and regenerative medicine therapies (Murry and Keller, 2008; Shahbazi and Zernicka-Goetz, 2018). Particularly, pluripotent stem cells can aggregate in three-dimensional culture and potentially reconstruct any organ when cultured under specific conditions. These organotypic structures, known as organoids, retain their organ identity and are genetically stable over long periods of time, thus representing a powerful tool to dissect the mechanisms underpinning development and for disease modeling (Lancaster and Knoblich, 2014).

To date, several signaling pathways that regulate ESC pluripotency have been identified. Leukemia inhibitory factor (LIF) and bone morphogenic protein (BMP) signaling are strongly involved in the maintenance of ESC pluripotency via the LIF receptor and BMP receptor families, respectively (Niwa et al., 2009; Ying et al., 2003). In contrast, fibroblast growth factor (FGF) signaling triggers ESC differentiation via the FGF receptor family (Lanner and Rossant, 2010). Wingless-type (Wnt) signaling has been identified as an essential pathway for maintaining pluripotency in ESCs via interaction of Wnt ligands with frizzled (Fzd) proteins, which are seven-transmembrane domain G-protein-coupled receptors (ten Berge et al., 2011). Enforced activation by Wnt through CHIR99201 (CHIR) in combination with the FGF signaling inhibitor PD0325901 (PD) is commonly used to culture ESCs in an undifferentiated state (Ying et al., 2008; Ying and Smith, 2017). However, Wnt activation requires complex signaling translation via a large family of protein ligands, receptors, co-receptors, agonists and antagonists; as a consequence, Wnt signaling regulation is still poorly understood. Indeed, in contrast to the generally accepted view of Wnt signaling, some studies have reported that Wnt activation results in ESC differentiation (He et al., 2008; Price et al., 2013; Zhang et al., 2013). In addition, Wnt signaling plays a crucial role in embryo development, tumor initiation, and organoid growth, maturation and morphogenesis (McCauley and Wells, 2017; Steinhart and Angers, 2018; Zhan et al., 2017). These observations emphasize the importance of clarifying the mechanisms that modulate Wnt signaling.

Mucin-type *O*-glycosylation (hereafter just referred to as *O*-glycosylation) is an evolutionarily conserved protein modification and, together with *N*-linked glycosylation, is one of the most abundant forms of glycosylation present on membrane proteins and secreted proteins (Tran and Ten Hagen, 2013). Indeed, 83% of human proteins are *O*-glycosylated (Steentoft et al., 2013). *O*-glycosylation is a stepwise process characterized by the initial attachment of *N*-acetylgalactosamine (GalNAc) to the hydroxyl group of serine or threonine residues of the target protein by a large family of up to 19 polypeptide α-*N*-acetylgalactosaminyltransferases (ppGalNAc-Ts) in mouse; the attachment of GalNAc forms the so-called Tn antigen (Fig. 1A). Galactose (Gal), sialic acid (NeuAc) or *N*-acetylglucosamine (GlcNAc) can be successively added to Tn antigen by core 1 β1,3-galactosyltransferase (C1GalT1), GalNAc α2,6-sialyltransferase-I (ST6GalNAc-I), and β1,3-*N*-

[1]Laboratory of Cell Biology, Department of Bioinformatics, Graduate School of Engineering, Soka University, 1-236 Tangi-machi, Hachioji, Tokyo 192-8577, Japan. [2]Department of Anatomy, Kyorin University School of Medicine, 6-20-2 Shinkawa, Mitaka, Tokyo 181-8611, Japan. [3]Department of Advanced Clinical Glycobiology, Faculty of Medicine and Graduate School of Medicine, Hokkaido University, Kita 15, Nishi 7, Kita-ku, Sapporo 060-8638, Japan. [4]Department of Pharmacy, Kinjo Gakuin University, 2-1723 Omori, Moriyama-ku, Nagoya, Aichi 463-8521, Japan. [5]Department of Molecular and Tumor Pathology, Graduate School of Medicine, Chiba University, 1-8-1 Inohana, Chuo-ku, Chiba 260-8670, Japan. [6]Glycan & Life System Integration Center (GaLSIC), Faculty of Science and Engineering, Soka University, 1-236 Tangi-machi, Hachioji, Tokyo 192-8577, Japan.

*Author for correspondence (shoko@soka.ac.jp)

F.P., 0000-0002-0347-379X; S.N., 0000-0002-1668-2603

Handling Editor: John Heath
Received 3 March 2020; Accepted 9 September 2020

Journal of Cell Science

Journal of Cell Science (2020) 133, jcs245845. doi:10.1242/jcs.245845

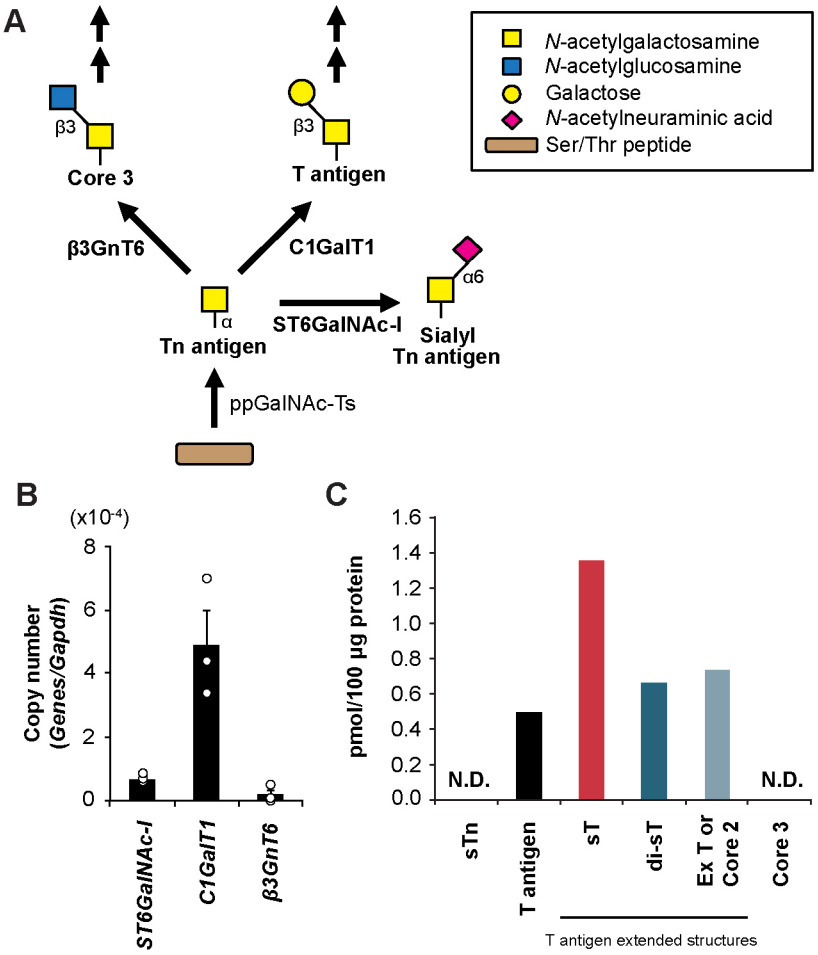

Fig. 1. The mucin-type *O*-glycosylation elongation pathway via C1GalT1 is the most prominent in ESCs. (A) Schematic diagram of mucin-type *O*-glycosylation pathway. (B) *ST6GalNAc-I*, *C1GalT1* and *β3GnT6* mRNA absolute quantification by real-time PCR. The gene copy number is normalized to that of *Gapdh*. The values are shown as the means±s.e.m. of three independent experiments. (C) Absolute amount of *O*-glycan structures detected by mass spectrometry in ESCs by MALDI-TOF MS. sTn, sTn antigen; Core 3, core 3 structure, T antigen, and C1GalT1-mediated elongation pathway modifications (sT, sT antigen; di-sT, disialyl T antigen; Ex T or Core 2, extended T antigen or core 2 structure). The data were obtained from a single technical and biological replicate. N.D., not detected.

acetylglucosaminyltransferase-6 (β3GnT6), to form three main structures – T antigen (Galβ1-3GalNAc), sialyl Tn antigen (NeuAcα2-6GalNAc) and the core 3 structure (GlcNAcβ1-3GalNAc) (Bennet et al., 2012). Several studies have demonstrated that *O*-glycosylation plays a vital role in development and tumorigenesis. The importance of this modification during embryonic development is highlighted by the fact that disruption of the *C1GalT1* gene causes embryonic lethality in mice (Xia and McEver, 2006). *Galnt1* is the most abundantly expressed of the 19 ppGalNAc-Ts during murine embryonic submandibular gland development; mice deficient for *Galnt1* show a reduction in FGF signaling (Tian et al., 2012). We previously reported that *O*-glycosylation is required for normal development in *Drosophila* (Fuwa et al., 2015; Itoh et al., 2016, 2018). Furthermore, aberrant glycoprofiles are observed in essentially all types of cancers (Pinho and Reis, 2015). Recently, a novel culture medium that includes the primitive growth factor $NME7_{AB}$, which binds to the extracellular domain of the cleaved form of the *O*-glycosylated protein MUC1, was shown to maintain human ESCs in an undifferentiated state (Carter et al., 2016), suggesting that *O*-glycosylation is involved in the pluripotency network. However, the function of *O*-glycosylation in ESC pluripotency network and its relationship to signaling in ESCs remain unknown.

The present study was initiated to clarify the role of mucin-type *O*-glycosylation in the ESC pluripotency network. We identified the most prominent mucin-type *O*-glycosylation elongation pathway in ESCs and manipulated the expression of the enzyme involved in its formation. Our results provide the first demonstration that *O*-glycosylation controls ESC pluripotency by directly regulating Wnt signaling receptor endocytosis.

RESULTS

The mucin-type *O*-glycosylation elongation pathway via C1GalT1 is the most prominent in ESCs

Tn antigen formation, which can be catalyzed by 19 different ppGalNAc-Ts in mouse, is the initial step of mucin-type *O*-glycosylation. Tn antigen is further elongated by ST6GalNAc-I, C1GalT1 or β3GnT6 to synthesize sTn antigen, T antigen or the core 3 structure, respectively (Fig. 1A). The partial functional redundancy of ppGalNAc-Ts makes analysis of their function highly complex (Bennet et al., 2012); we therefore focused on the catalyzation step following Tn antigen formation that is selectively performed by ST6GalNAc-I, C1GalT1 or β3GnT6. In addition to sTn antigen, T antigen and the core 3 structure, the Tn antigen can also be extended to form core 5 to 8 structures. However, core 5 to 8 structures have an extremely restricted occurrence and the glycosyltransferases involved in their formation remain to be fully characterized (Brockhausen et al., 2009); thus, they are not considered in this study.

We analyzed mRNA expression in ESCs and found that *C1GalT1* was the most highly expressed of the three enzymes (Fig. 1B). Quantitative analysis of *O*-glycans in ESCs was performed by mass spectrometry using optimized microwave-assisted β-elimination in the presence of a pyrazolone (BEP) method for *O*-glycomic analysis that was validated with a mixture of equal quantities of four glycans

Journal of Cell Science (2020) 133, jcs245845. doi:10.1242/jcs.245845

(Furukawa et al., 2015a). We here identified T antigen, and its further modifications, as the only detectable structure among sTn antigen, T antigen and the core 3 structure (Fig. 1C). Interestingly, the absolute amount of T antigen, and C1GalT1-mediated elongation pathway modifications, were consistent among different ESC lines, suggesting that the C1GalT1 elongation pathway might play a crucial role in ESCs (Fig. S1A,B). Next, we investigated the *O*-glycosyltransferase dynamics during early and late differentiation by using an embryoid body (EB) assay. *C1GalT1* showed the highest level of expression among the three *O*-glycosyltransferases between day 0 and day 4, suggesting that the C1GalT1-mediated elongation pathway might have a role during early differentiation of ESCs. However, at later differentiation stages, expression of all three enzymes increased dramatically, indicating that the ESC surface might be decorated by several types of *O*-glycan structure during late differentiation (Fig. 1B; Fig. S1C–E).

C1GalT1 knockdown causes ESCs to exit from pluripotency

To elucidate the role of the C1GalT1 elongation pathway in determining pluripotency, we performed a RNAi knockdown (KD) of *C1GalT1*. Two constructs were designed that expressed different siRNAs targeting *C1GalT1* (*C1GalT1* KD 1 and *C1GalT1* KD 2). At 4 days after transfection, *C1GalT1* KD cells showed decreased *C1GalT1* expression (Fig. 2A) followed by a reduction of T antigen at the cell membrane and internally, as shown by peanut agglutinin lectin (PNA) staining, which binds specifically to T antigen (Fig. 2B–F). *C1GalT1* KD resulted in a significant increase in Tn antigen and a mild decrease in sTn antigen at the cell surface, as shown by *Helix pomatia* agglutinin lectin (HPA) and *Sambucus nigra* lectin (SNA) staining, respectively (Fig. S2A–D). *C1GalT1* KD cells exhibited a flat shape, which is typical of differentiated cells, compared to the dome-shape morphology of undifferentiated cells (Fig. 3A); this observation demonstrated that *C1GalT1* KD cells were differentiated cells. Next, we analyzed the expression of the core pluripotency markers Oct3/4 (also known as POU5F1) and Sox2, and of SSEA-1, a pluripotent cell surface marker (Nakai-Futatsugi and Niwa, 2013). The levels of *Oct3/4* and *Sox2* mRNAs were significantly decreased in *C1GalT1* KD cells compared to the control; a similar decrease at the protein level was also observed (Fig. 3B–D). The SSEA-1^{+} cell population was reduced in *C1GalT1* KD cells compared to the control (Fig. 3E). To assess the ability of *C1GalT1* KD cells to self-renew, we performed a clonogenicity assay at 4 days post transfection. The number of alkaline phosphatase (ALP)-positive colonies was markedly decreased in *C1GalT1* KD cells, demonstrating that the self-renewing ability of *C1GalT1* KD cells was compromised (Fig. 3F). ESC pluripotency and self-renewal loss following *C1GalT1* KD was further confirmed by using stable *C1GalT1* KD ESCs (Fig. S3A–D). An analysis of the expression of differentiation markers showed that *C1GalT1* KD resulted in an upregulation of the trophoblast markers *Cdx2* and *Gata3*, suggesting that *C1GalT1* KD induces ESC

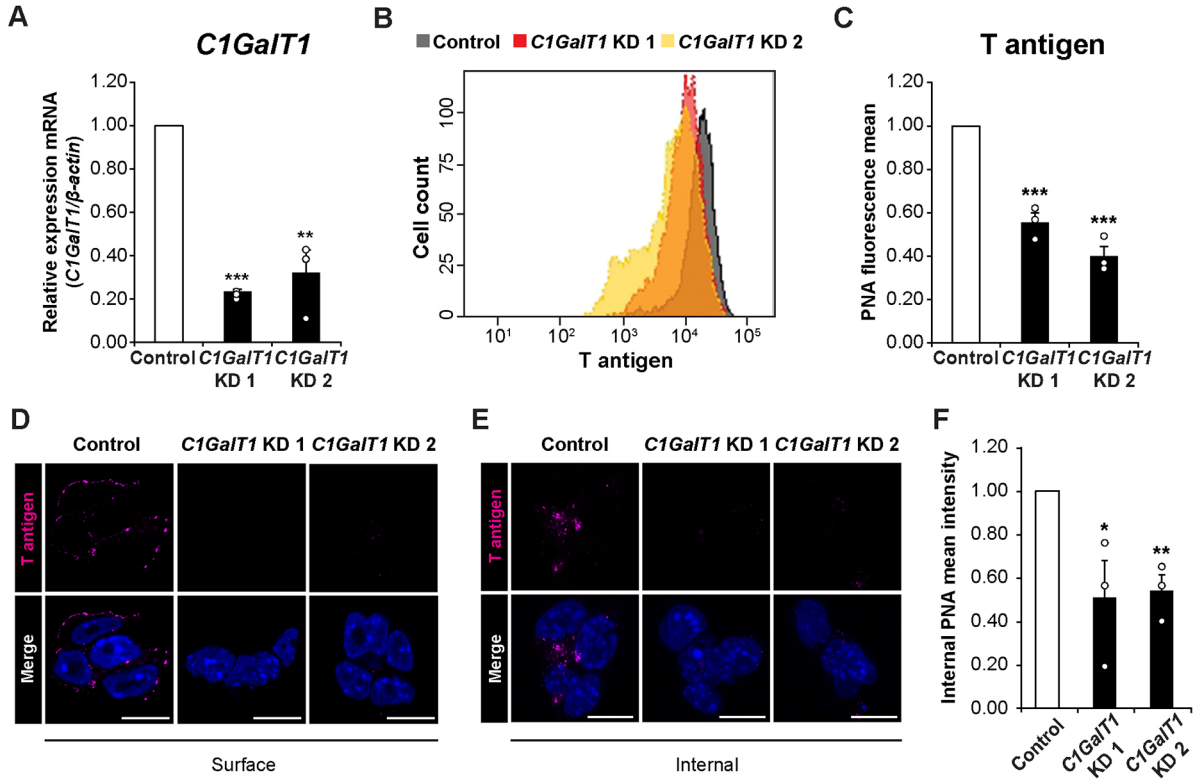

Fig. 2. Knockdown of *C1GalT1* results in T antigen reduction. (A) Real-time PCR analysis of *C1GalT1* KD cells. The amount of *C1GalT1* was normalized against that of β-actin. (B) FACS analysis of *C1GalT1* KD cells stained by PNA–FITC. (C) Histogram representing fluorescence mean intensity of data in B. The fold change is presented relative to that of control cells. (D) Representative image of cell surfaces of *C1GalT1* KD cells after immunostaining using PNA–biotin. Nuclei were stained with Hoechst. Scale bars: 10 µm. (E) Representative image of a maximum intensity projection of internal molecules in *C1GalT1* KD cells after immunostaining using PNA–biotin. Nuclei were stained with Hoechst. Scale bars: 10 µm. (F) Internal PNA mean intensity of images in E. The mean intensity is shown as fold change relative to that of the control. Quantitative values are shown as means±s.e.m. of three independent experiments. **P*<0.05; ***P*<0.01; ****P*<0.001 (unpaired two-tailed Student's *t*-test).

Journal of Cell Science (2020) 133, jcs245845. doi:10.1242/jcs.245845

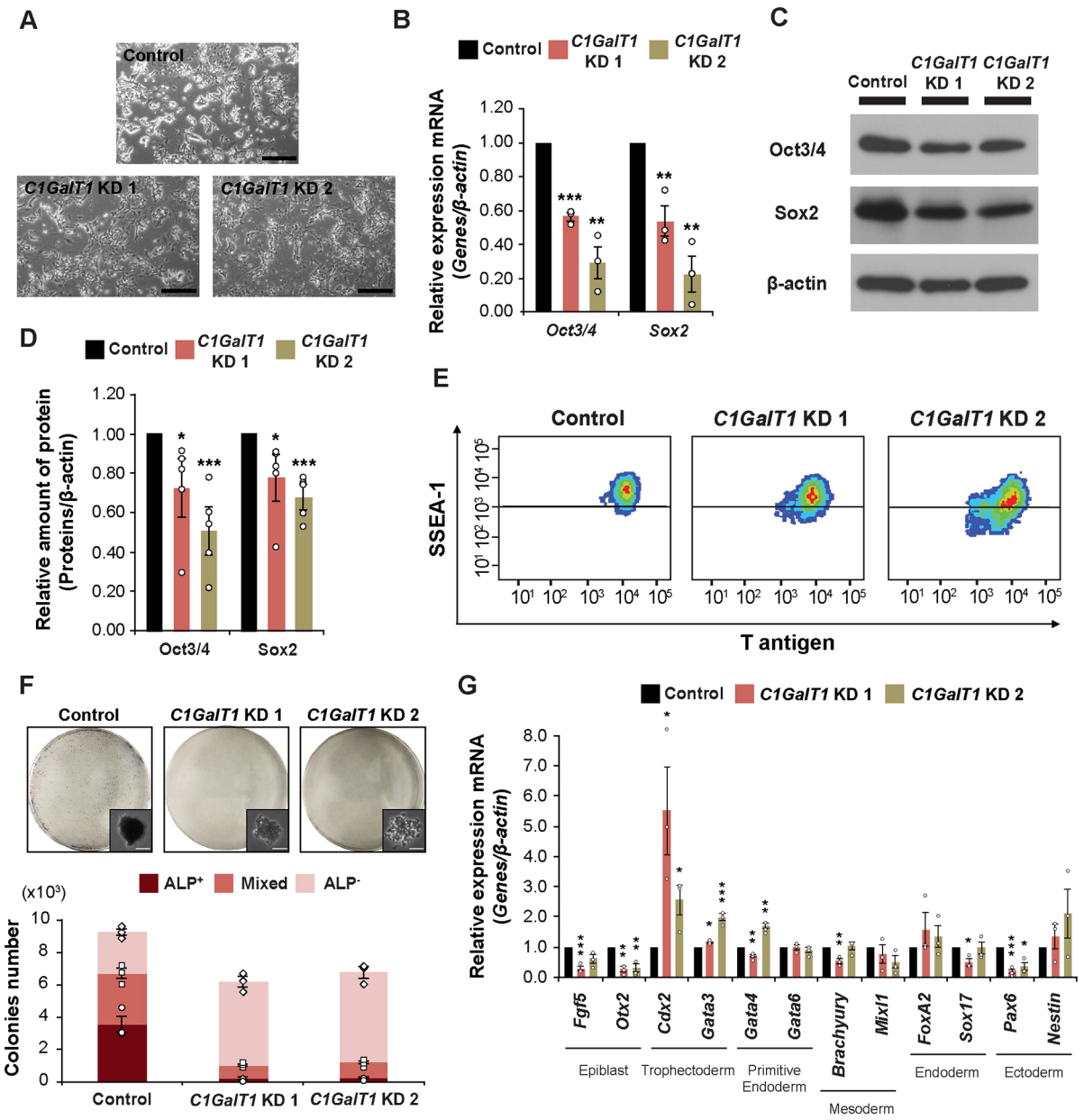

Fig. 3. Knockdown of *C1GalT1* promotes exit from the pluripotent state. (A) Morphology of control (upper panel), *C1GalT1* KD 1 (left panel), and *C1GalT1* KD 2 (right panel) cells. Scale bars: 200 µm. (B) Real-time PCR analysis of the pluripotent markers *Oct3/4* and *Sox2* in *C1GalT1* KD cells normalized against β-actin and shown as fold change relative to control cells. (C) Representative image of a western blot analysis (n=5) of pluripotent markers Oct3/4 and Sox2 in *C1GalT1* KD cells. (D) The band intensities of Oct3/4 and Sox2 in image C were normalized against β-actin and shown as a fold change relative to control cells. (E) Density plot by FACS analysis of *C1GalT1* KD cells stained with anti-SSEA-1–PE Ab and PNA–FITC. The dark line separates the SSEA-1$^+$ population (upper side) and the SSEA-1$^-$ population (lower side). (F) Clonogenicity assay of *C1GalT1* KD cells. Scale bars: 25 µm. (G) Real-time PCR analysis of differentiation markers in *C1GalT1* KD cells normalized against β-actin and shown as a fold change relative to control cells. Quantitative values are shown as means±s.e.m. from three (B,F,G) or five (D) independent experiments. *P<0.05; **P<0.01; ***P<0.001 (unpaired two-tailed Student's t-test).

transdifferentiation toward the trophectoderm (Fig. 3G). Consistent with this, an EB assay showed an enhanced differentiation potential in *C1GalT1* KD ESCs (Fig. S3E,F). These data demonstrate that *C1GalT1* KD cells spontaneously exit from pluripotency, even in the presence of LIF.

C1GalT1 knockdown promotes canonical Wnt signaling in ESCs

Previous studies have reported that mucins, which are heavily *O*-glycosylated proteins, interact with β-catenin, the key mediator of the canonical Wnt signaling, during many malignancies (Pai et al., 2016). Therefore, we hypothesized that *C1GalT1* KD might alter canonical Wnt signaling in ESCs. Activation of Wnt signaling results in inhibition of β-catenin phosphorylation, thereby preventing its degradation. Stabilized β-catenin accumulates in the cytoplasm and translocates to the nucleus where, together with Tcf/Lef, it triggers Wnt-specific target gene transcription (Nusse and Clevers, 2017). Here, we found that *C1GalT1* KD cells exhibited a reduction in phospho-β-catenin (p-β-catenin) and an increase in total β-catenin (Fig. 4A,B). A reduction in the level of β-catenin mRNA was observed, suggesting that *C1GalT1* KD resulted in increased β-catenin protein stability (Fig. 4C). A luciferase assay

Journal of Cell Science (2020) 133, jcs245845. doi:10.1242/jcs.245845

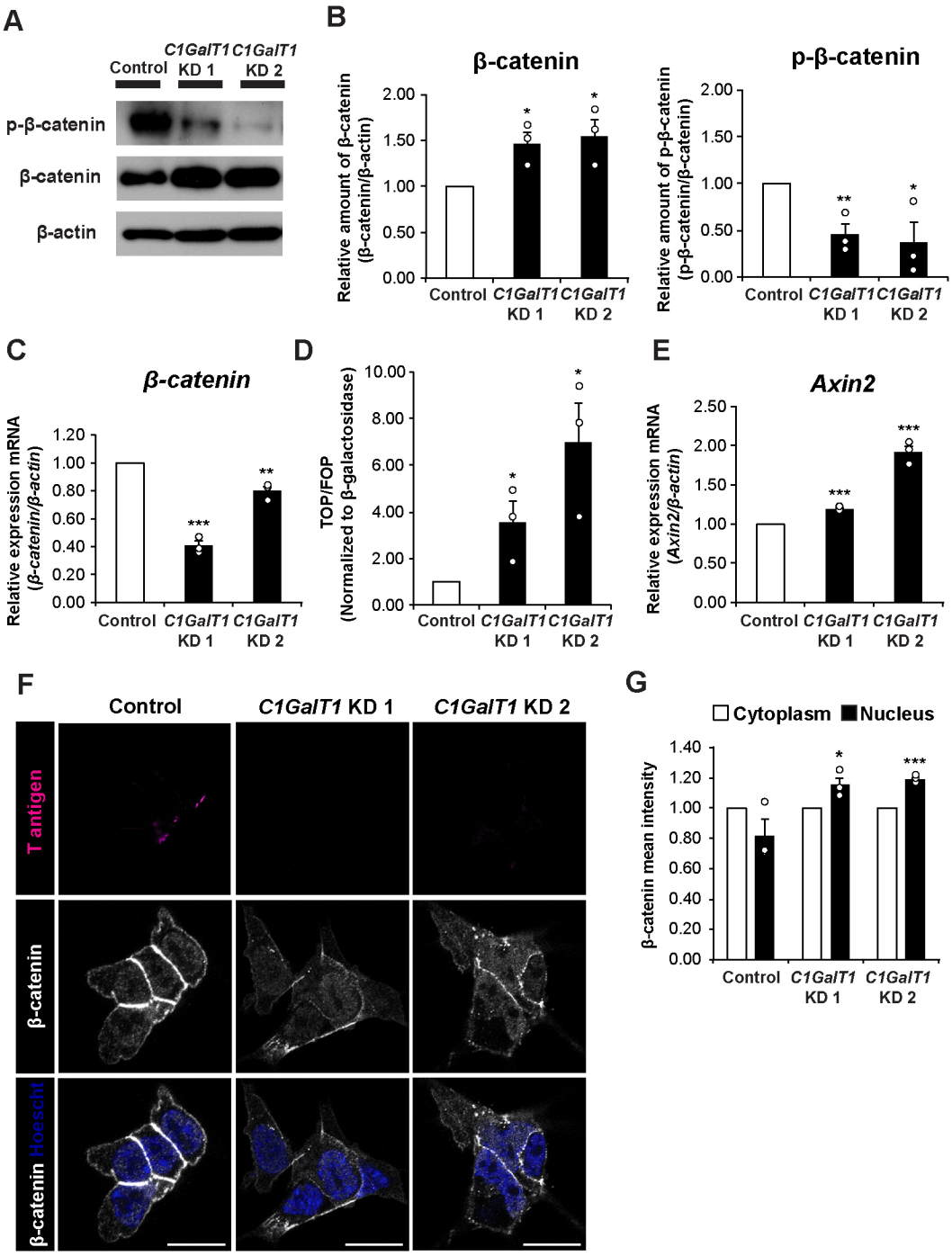

Fig. 4. Knockdown of *C1GalT1* enhances canonical Wnt signaling activation. (A) Representative image of western blot analysis (n=3) using antibodies against p-β-catenin and β-catenin in *C1GalT1* KD cells. (B) β-catenin and p-β-catenin western blot band intensities normalized against β-actin and β-catenin, respectively, and shown as fold change relative to control cells. (C) Real-time PCR analysis of β-catenin in *C1GalT1* KD cells normalized against β-actin levels and shown as a fold change relative to control cells. (D) Luciferase assay of *C1GalT1* KD cells. The relative light unit amount is shown as a ratio of TOPFLASH: FOPFLASH normalized against β-galactosidase and shown as a fold change relative to control cells. (E) Real-time PCR analysis of *Axin2* in *C1GalT1* KD cells normalized against β-actin and shown as a fold change relative to control cells. (F) Representative image (n=3) of intracellular molecules using PNA–biotin and an anti-β-catenin Ab in *C1GalT1* KD cells. Nuclei were stained with Hoechst. Scale bars: 10 µm. (G) Cytoplasmic and nuclear β-catenin mean intensity of *C1GalT1* KD cells. The mean intensity is shown as fold change relative to cytoplasmic β-catenin of each sample. Quantitative values are shown as means±s.e.m. of three independent experiments. *P<0.05; **P<0.01; ***P<0.001 (unpaired two-tailed Student's t-test).

using a β-catenin/Tcf responsive element (TOP) showed marked upregulation of Wnt signaling (Fig. 4D), followed by an increased expression of the Wnt-specific target gene *Axin2* (Fig. 4E). Moreover, immunostaining using an anti-β-catenin antibody (Ab) in permeabilized *C1GalT1* KD cells showed an increased localization of β-catenin in the nucleus compared to what was seen in the control (Fig. 4F,G). These results demonstrate that *C1GalT1* KD promotes canonical Wnt signaling activation in ESCs.

Journal of Cell Science (2020) 133, jcs245845. doi:10.1242/jcs.245845

Mucins have also been reported to activate phosphoinositide 3-kinase (PI3K)/Akt and Fgf signaling in breast cancer cells (Woo et al., 2012; Hiraki et al., 2016). However, *C1GalT1* KD did not result in activation of PI3K/Akt and Fgf signaling pathways in ESCs (Fig. S4A–D). Previously published ChIP-seq analysis of wild-type, untreated ESCs [available at NCBI Sequence Read Archive; accession numbers: SRX1204276 (Dahl et al., 2016), SRX191012 (Mouse ENCODE et al., 2012) and SRX1080398 (Wang et al., 2017)] revealed the following characteristics in the *C1GalT1* promoter region: an active promoter as shown by the presence of the marker H3K4me3 (Tserel et al., 2010), an open conformation as shown by DNase-seq, and a Wnt effector as shown by Tcf3 binding (Fig. S4E). These findings suggest that Wnt signaling may regulate *C1GalT1* expression (Oki et al., 2018).

Fzd5 carries T antigen

Canonical Wnt signaling is initiated by the binding of the Wnt ligand to its Fzd receptors, which in turn dimerize with the co-receptor LRP5–LRP6 and results in downstream signaling (Nusse and Clevers, 2017). Among the Fzd receptor family involved in the canonical Wnt signaling in ESCs, *Fzd5* is the most highly expressed and plays an essential role during development (Hao et al., 2006). Support for this conclusion comes from the fact that *Fzd5* depletion causes embryonic lethality in mice (Ishikawa et al., 2001). Here, to investigate whether Wnt signaling receptors are *O*-glycosylated, we precipitated Fzd5 as a putative candidate. A pulldown assay using biotinylated PNA followed by western blotting using an anti-Fzd5 Ab showed that Fzd5 was successfully precipitated, and demonstrated that Fzd5 carries T antigen (Fig. 5A). Next, we performed an immunoprecipitation analysis on an ESC lysate using an anti-Fzd5 Ab. A lectin blot analysis of the immunoprecipitates using PNA confirmed that Fzd5 was modified by T antigen (Fig. 5B). Moreover, the amount of Fzd5 protein precipitated in *C1GalT1* KD cells decreased compared to the control, further confirming that Fzd5 is *O*-glycosylated (Fig. 5C,D). However, T antigen was not detected by lectin blot analysis for LRP5 and LRP6 immunoprecipitates, demonstrating that the Fzd co-receptors LRP5 and LRP6 do not carry T antigen (Fig. S5). Together, these results demonstrate, for the first time, that Wnt receptor Fzd5 carries T antigen. Thus, other Fzd receptors, including secreted Fzd molecules, may also be *O*-glycosylated.

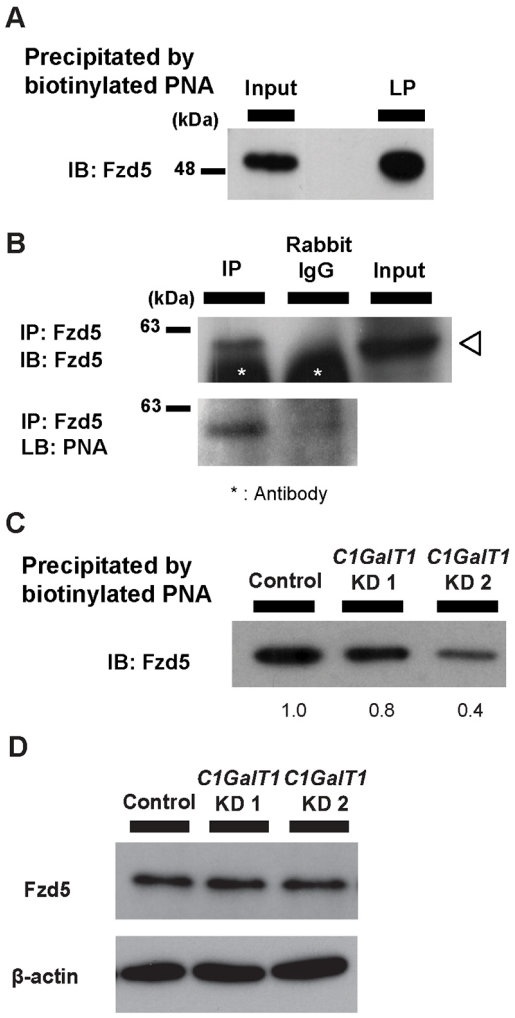

Fig. 5. Fzd5 carries T antigen. (A) Representative image of a western blot (IB) using an anti-Fzd5 Ab on the lectin-precipitated fraction (LP) precipitated with biotinylated PNA. The input represents the total ESC lysate. Similar results were obtained in four independent experiments. (B) Representative image of a western blot (IB) using an anti-Fzd5 Ab and lectin blot (LB) by PNA–HRP on the immunoprecipitated fraction (IP) precipitated with an antibody against Fzd5. The input represents the total ESC lysate. The arrowhead indicates the Fzd5 protein. Similar results were obtained in three independent experiments. (C) Representative image of a western blot (IB) using an anti-Fzd5 Ab on the lectin precipitated fraction precipitated with biotinylated PNA in *C1GalT1* KD cells. Similar results were obtained in three independent experiments. Band intensity fold change relative to control is shown below the western blot image. (D) Representative image of western blot using an anti-Fzd5 Ab in *C1GalT1* KD cells. Similar results were obtained in three independent experiments.

T antigen on Fzd5 regulates its galectin-3-mediated endocytosis

O-glycosylation has multiple functions, such as in protein–protein interaction, and in trafficking and turnover of cell surface proteins (Razawi et al., 2013; Karabasheva et al., 2014). We therefore analyzed the role of T antigen on Fzd5. Immunostaining using an anti-Fzd5 Ab in permeabilized *C1GalT1* KD cells revealed that there was a striking reduction of internalized Fzd5, as shown by puncta staining, compared with what was seen in the control (Fig. 6A–C; Movies 1–3). In contrast, Fzd5 staining at the cell surface increased in *C1GalT1* KD cells (Fig. 6D). A surface biotinylation assay indicated that Fzd5 was markedly increased on the surface of *C1GalT1* KD cells (Fig. 6E). Moreover, ultrastructural localization of Fzd5 by immunoelectron microscopy showed that colloidal gold labeling was scarcely present on the plasma membrane of control cells compared to in *C1GalT1* KD cells (Fig. 6F), further demonstrating that Fzd5 is retained at the cell membrane after *C1GalT1* KD. To confirm these observations, we treated ESCs with the *O*-glycosylation inhibitor benzyl 2-acetoamido-2-deoxy-α-D-galactopyranoside (GalNAc-Bn) and then stained the cells using an anti-Fzd5 Ab. A similar effect was found to that seen in *C1GalT1* KD cells; namely, we observed a dramatic reduction of internalized Fzd5 and an increase at the cell surface after *O*-glycosylation inhibition (Fig. S6A–D; Movies 4 and 5). These observations confirmed that T antigen on Fzd5 is involved in Fzd5 internalization. The ultrastructural localization of Fzd5 was investigated using two different Abs against Fzd5. Colloidal gold labeling was observed inside and outside the endosomes of control cells, as shown by using anti-Fzd5 Abs against the N-terminal and C-terminal regions, respectively (Fig. 6G). In addition, immunostaining showed that the early endosome marker Rab5 colocalized with Fzd5 in ESCs (Fig. 6H; Movie 6), demonstrating that Fzd5 is cleared from the plasma membrane by endocytosis.

Journal of Cell Science (2020) 133, jcs245845. doi:10.1242/jcs.245845

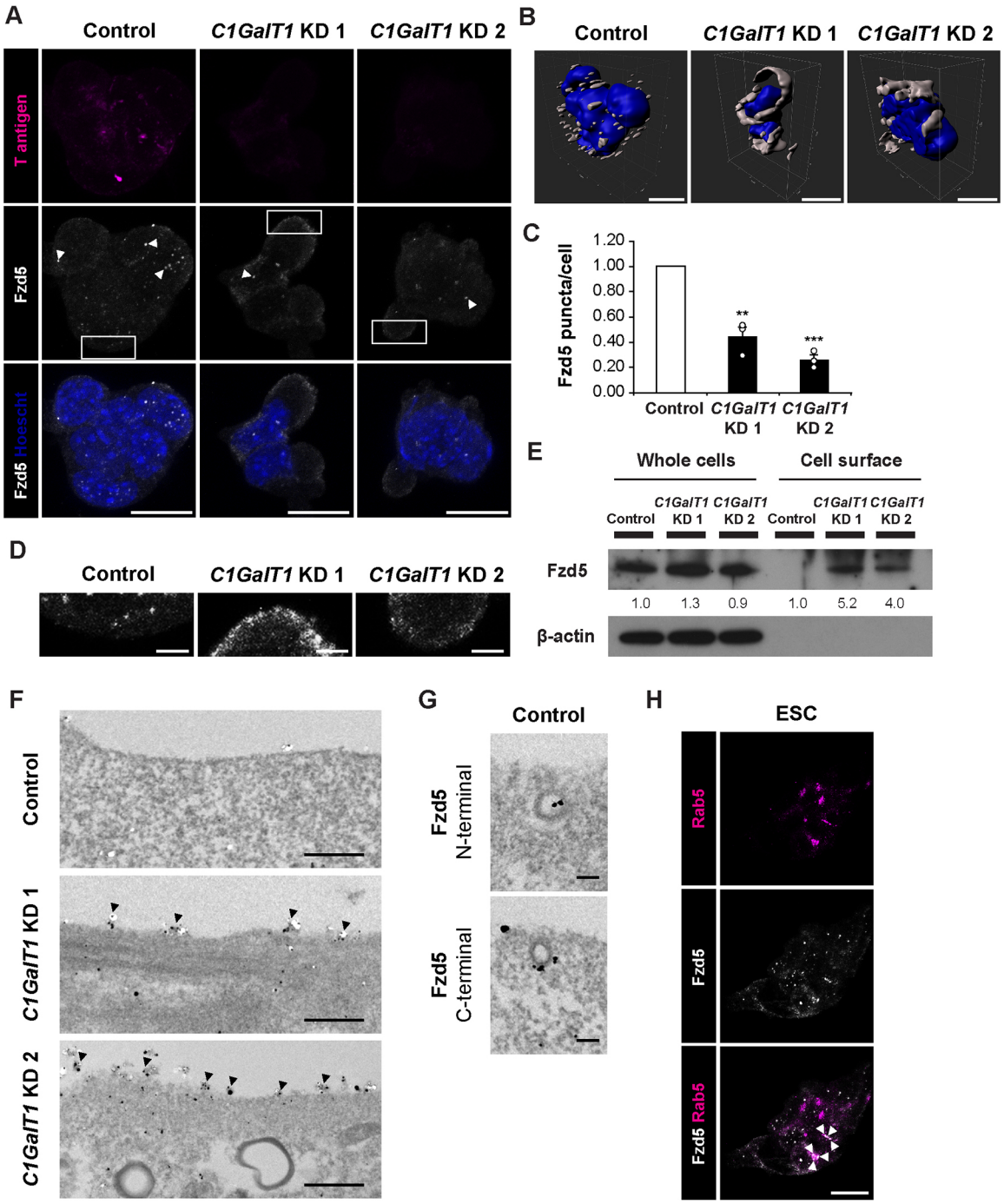

Fig. 6. T antigen on Fzd5 regulates its endocytosis. (A) Representative image (n=3) of a maximum intensity projection of intracellular molecules using PNA–biotin and an anti-Fzd5 Ab in *C1GalT1* KD cells. Nuclei were stained with Hoechst. Arrowheads indicate Fzd5 puncta staining. Scale bars: 10 µm. (B) 3D reconstruction of images in A using Imaris version 9.3.1. Scale bars: 10 µm. (C) Quantification of Fzd5 puncta staining normalized against the number of nuclei and shown as a fold change relative to control. (D) Magnification of areas highlighted in A. Scale bar: 2.5 µm. (E) Assessment of Fzd5 surface protein in *C1GalT1* KD cells using a biotinylation assay. Band intensity fold change relative to control is shown below the western blot image. Representative of three independent experiments. (F) Representative transmission electron micrographs from *C1GalT1* KD cells. Arrowheads indicate Fzd5 staining at the plasma membrane. Scale bars: 500 nm. The micrographs were obtained from a single biological replicate. (G) Representative transmission electron micrographs from control cells showing the ultrastructural localization of Fzd5 in the endosome. Colloidal gold labeling is inside the endosome using an anti-Fzd5 Ab against the N-terminal region (upper panel), and outside the endosome using an anti-Fzd5 Ab against the C-terminal region (lower panel). Scale bars: 10 nm. The micrographs were obtained from a single biological replicate. (H) Representative image (n=3) of a maximum intensity projection of intracellular molecules using an anti-Fzd5 Ab and an anti-Rab5 Ab in ESCs. Arrowheads indicate colocalization of Fzd5 puncta and Rab5. Scale bars: 10 µm. Quantitative values are shown as means±s.e.m. of three independent experiments. **P<0.01; ***P<0.001 (unpaired two-tailed Student's t-test).

Galectins (Lgals) belong to a family of carbohydrate-binding proteins that bind to β-galactose-containing glycoproteins (Johannes et al., 2018). Previous studies have reported that Lgals, in particular Lgals3, have a stimulatory effect on endocytosis (Merlin et al., 2011; Gao et al., 2012; Lepur et al., 2012; Lakshminarayan et al., 2014). Moreover, frontal affinity

Journal of Cell Science (2020) 133, jcs245845. doi:10.1242/jcs.245845

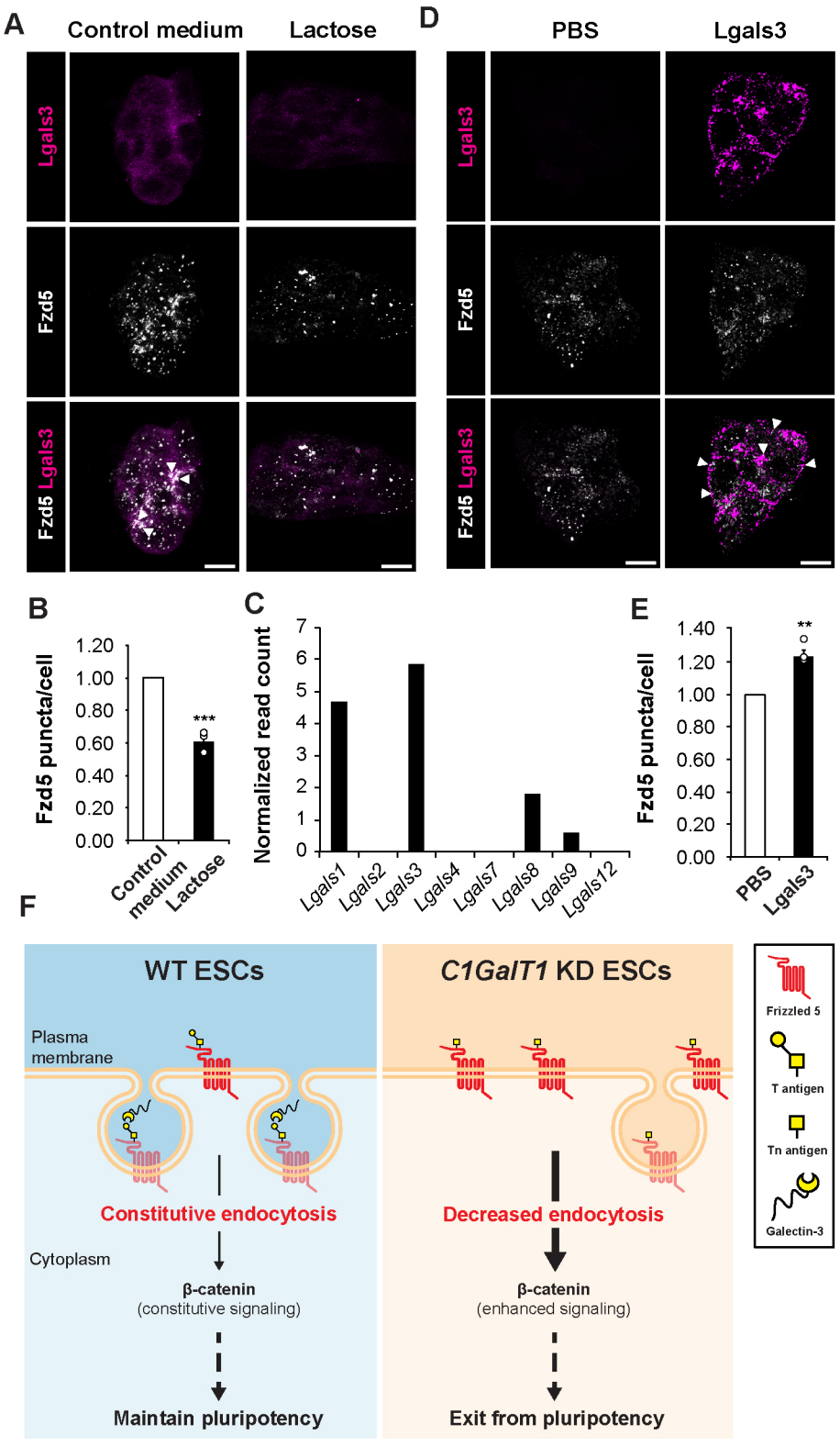

Fig. 7. Fzd5 endocytosis is mediated by galectin-3. (A) Representative image (n=3) of a maximum intensity projection of intracellular molecules using an anti-Fzd5 Ab and an anti-Lgals3 Ab in ESCs treated with 50 mM lactose monohydrate for 30 min. Arrowheads indicate colocalization of Fzd5 puncta and Lgals3. Scale bars: 10 µm. (B) Quantification of Fzd5 puncta staining of image in A normalized against the number of nuclei and shown as a fold change relative to control. (C) Galectin expression in ESCs analyzed by RNA-seq shown as normalized read count. RNA-seq data were obtained from a single technical and biological replicate. (D) Representative image (n=3) of a maximum intensity projection of intracellular molecules using an anti-Fzd5 Ab and an anti-Lgals3 Ab in ESCs treated with 15 µg/ml of recombinant Lgals3 for 30 min. Arrowheads indicate colocalization of Fzd5 puncta and Lgals3. Scale bars: 10 µm. (E) Quantification of Fzd5 puncta staining in image D normalized against the number of nuclei and shown as a fold change relative to control. Quantitative values are shown as means±s.e.m. of three independent experiments. $^{**}P$<0.01 and $^{***}P$<0.001 (unpaired two-tailed Student's t-test). (F) Schematic representation of ESC pluripotency regulation by mucin-type O-glycosylation. Mucin-type O-glycosylated Wnt receptor Fzd5 on wild-type (WT) ESCs is cleared from the plasma membrane by endocytosis via the binding of galectin-3 to T antigen, resulting in constitutive β-catenin signaling, which promotes the maintenance of ESC pluripotency. By contrast, *C1GalT1* KD ESCs show disrupted galectin-3-mediated endocytosis of Fzd5 leading to its retention at the plasma membrane. As a result, Wnt signaling, mediated by β-catenin, is enhanced and culminates in the loss of ESC pluripotency.

chromatography analysis has demonstrated that T antigen is a ligand for Lgals9, followed by Lgals2, Lgals3 and Lgals4 (Iwaki and Hirabayashi, 2018). Therefore, we hypothesized that Lgals are involved in Fzd5 endocytosis. Immunostaining using an anti-Fzd5 Ab in permeabilized ESCs showed a marked reduction of internalized Fzd5 in ESCs treated with a high concentration of lactose, demonstrating that Lgals regulate Fzd5 endocytosis (Fig. 7A,B). RNA-seq analysis showed that, among the Lgals that can bind T antigen, *Lgals3* was the most highly expressed in ESCs (Fig. 7C). Consistent with this, addition of Lgals3 resulted in an enhancement of internalized Fzd5, confirming that Lgals3 is involved in Fzd5 endocytosis in ESCs (Fig. 7D,E; Movie 7). The cell surface E3 ubiquitin ligase Znrf3 and its homolog Rnf43 inhibit Wnt signaling by targeting surface-expressed Fzd to lysosomes in

human embryonic kidney cells and mouse intestinal stem cells (Hao et al., 2012; Koo et al., 2012). Thus, reduction of T antigen on Fzd5 may alter its interaction with Znrf3 and/or Rnf43, prolonging Wnt receptor availability at the cell surface. RNA-seq analysis showed that *Znrf3* is highly expressed in ESCs compared to *Rnf43* (Fig. S7A). However, *Znrf3* knockdown in ESCs did not affect Fzd5 endocytosis (Fig. S7B–D). In conclusion, our findings demonstrate that reduction of T antigen results in disruption of Lgals3-mediated endocytosis of the Wnt receptor Fzd5. As a result, Fzd5 is retained at the plasma membrane, thereby prolonging the activation of Wnt signaling (Fig. 7F).

DISCUSSION

It is becoming clear that glycosylation acts as a pivotal regulatory switch of pluripotency in a range of cell types in different organisms (Nishihara, 2018). In the present study, we characterized the function of mucin-type *O*-glycosylation in the pluripotency. network and clarified the relationship between *O*-glycosylation and signaling in ESCs. The C1GalT1-mediated elongation pathway is the most prominent in ESCs. Knockdown of *C1GalT1* expression results in a decrease of T antigen on the Wnt receptor Fzd5, reducing the level of Lgals3-mediated Fzd5 endocytosis. The retention of Fzd5 on the surface, in turn, promotes excessive canonical Wnt signaling activation via β-catenin stabilization, resulting in the exit from pluripotency (Fig. 7F).

The expression of *O*-glycosyltransferases increases after ESC differentiation into embryoid bodies (EBs) or extraembryonic endoderm cells, suggesting that *O*-glycosylation may play a key role during early commitment (Nairn et al., 2012). A recent study has shown that *O*-glycosylation plays a critical role in maintaining the epithelial state of trophoblast stem cells, which are derived from the first embryo lineage commitment (Raghu et al., 2019). Here, we demonstrated that *O*-glycosylation is crucial for the maintenance of ESC pluripotency; our findings provide further insights into the roles of *O*-glycosylation in early embryonic development. Furthermore, we showed that *C1GalT1* was most highly expressed during early commitment in ESCs (Fig. 1B; Fig. S1C–E) and that *C1GalT1* KD induced expression of the trophectoderm markers *Cdx2* and *Gata3* (Fig. 3G). Thus, it will be of particular interest to investigate the role of mucin-type *O*-glycosylation in the early commitment of ESCs and in early embryo development *in vivo*.

A previous comprehensive study of the glycomes of various cell lines reported that the T antigen elongation pathway is the most prominent in conventional human ESCs, similar to what is found in mouse ESCs (Fujitani et al., 2013). However, mouse and conventional human ESCs reflect two different pluripotent states, namely the naïve and the primed state, respectively, which rely on different signaling pathways to maintain the pluripotent state and induce differentiation (Weinberger et al., 2016). Thus, the influence of T antigen on the pluripotency network and differentiation potential is likely to differ between mouse and human ESCs. Currently, we are exploring the role of C1GALT1-mediated elongation pathway in the conventional human ESC pluripotency network.

In the past decade, Wnt signaling has been shown to be a key factor in the maintenance of the undifferentiated state. The addition of Wnt3a and LIF is sufficient to support self-renewal and allows derivation of ESCs from non-permissive strains (ten Berge et al., 2011). The induction of Wnt signaling through treatment with CHIR together with the FGF signaling inhibitor PD is commonly used to maintain the undifferentiated state in cultured ESCs (Ying et al., 2008; Ying and Smith, 2017). However, the Wnt signaling outcome depends on its interactions with other signaling pathways. CHIR alone induces ESC differentiation (Ying et al., 2008). In addition, other groups have reported that β-catenin promotes the expression of genes associated with both pluripotency and differentiation (Kelly et al., 2011; Price et al., 2013; Zhang et al., 2013). Therefore, Wnt signaling maintains cells in the undifferentiated state while at the same time priming cells for differentiation. Here, Wnt signaling dysregulation led to a loss of ESC pluripotency. Our previous study characterized the role of heparan sulfate proteoglycans in Wnt signaling regulation in ESCs (Sasaki et al., 2008). The present study identifies another mechanism through which glycosylation regulates Wnt signaling.

Mucin-type *O*-glycosylation plays multiple roles, including protection from shedding, protein–protein interactions, and protein turnover and trafficking (Tian and Ten Hagen, 2009; Razawi et al., 2013; Karabasheva et al., 2014). In this study, we demonstrated that T antigen on the Wnt receptor Fzd5 modulates endocytosis of Fzd5 via Lgals3 (Fig. 7F). Fzd endocytosis modulates Wnt signaling positively or negatively depending on the cellular context (Brunt and Scholpp, 2018). In the present study, a reduction in Fzd5 endocytosis resulted in Wnt signaling activation. Abnormalities in *O*-glycosylation and Wnt signaling are hallmarks of tumorigenesis (Pinho and Reis, 2015; Zhan et al., 2017). Here, we demonstrated for the first time a direct connection between *O*-glycosylation and Wnt signaling.

Pluripotent stem cell-derived organoids are a valuable tool for investigating the mechanisms of development and for disease modeling (Lancaster and Knoblich, 2014). However, improving organoid maturity remains one of the greatest challenges in this field. Recent studies identified Wnt as one of the central signaling molecules in organoid growth, patterning and morphogenesis (McCauley and Wells, 2017). In the present study, we identified a novel Wnt signaling regulatory mechanism regulated by mucin-type *O*-glycosylation, providing an additional approach of manipulation of organoid culture conditions. It will be of particular interest to understand the mechanistic role of mucin-type *O*-glycosylation with regard to Wnt signaling during organoid maturation. In conclusion, our observations provide a significant contribution to research in developmental biology and to the development of future therapeutic applications.

MATERIALS AND METHODS

Cell culture

R1 (Nagy et al., 1993) and E14TG2a (Smith and Hooper, 1987) ESC lines were maintained on mouse embryonic fibroblasts that were prepared from embryos at embryonic day (E)14.5 and inactivated with 10 µg mitomycin C (Sigma-Aldrich). The cell lines were maintained in ESC medium, consisting of DMEM (Gibco) supplemented with 15% fetal bovine serum (FBS) (Nichirei Biosciences), 1% penicillin/streptomycin (Gibco), 0.1 mM 2-mercaptoethanol (Gibco), 0.1 mM nonessential amino acids (Gibco) and 1000 U/ml LIF (Chemicon International). The R1 ESC line was used for the experiments unless stated otherwise. ESC lines were recently tested for mycoplasma contamination and authenticated by ATCC cell line authentication service - mouse STR profiling.

To induce embryoid body (EB) formation, ESCs were transferred to 35-mm Low Cell Binding dishes (Nunc) and cultured in ESC medium in absence of LIF for 2.5, 4, 8 or 12 days. The EB assay from transient *C1GalT1* KD ESCs was performed 2 days post transfection and cells were collected at day 0 (ESCs), 2, 3, and 4.

For knockdown (KD) of the *C1GalT1* and *Znrf3* genes in ESCs, we generated small hairpin RNA (shRNA) expression vectors targeting two different regions of each gene [and also enhanced green fluorescent protein (*Egfp*) as the control] by inserting the appropriate double-stranded DNA between the BamH1 and HindIII sites of pSilencer 3.1-H1 (Ambion) or

Journal of Cell Science (2020) 133, jcs245845. doi:10.1242/jcs.245845

p.SUPER.retro.puro (OligoEngine), for transient and stable KD, respectively. shRNA sequences used for RNA interference (RNAi) were designed as described previously (Sasaki et al., 2009) using siDirect (https://sidirect.jp/esd/modules/modsiperfect/) and were as follows: *Egfp*, 5′-GATCCCGCCACAACGTCTATATCATGGGGAAAATCCATGATATAGACGTTGTGGCTTTTTTGGAAA-3′; *C1GalT1* KD 1, 5′-GATCCCGGGCCCAGCGTTGTAATAAAGGCTTCCTGTCACCTTTATTACAACGCTGGGCCCTTTTTTA-3′; *C1GalT1* KD 2, 5′-GATCCCGGCTTCTATCAAAGTATAACCGCTTCCTGTCACGGTTATACTTTGATAGAAGCCTTTTTTA-3′; *Znrf3* KD 1, 5′-GATCCCGCAACGTCGTAGTCAGAATGCTTCCTGTCACATTCTGACTACGACGTTGCTTTTTTA-3′; *Znrf3* KD 2, 5′-GATCCCCCAGAAAGTTCAACTCCAAGCTTCCTGTCACTTGGAGTTGAACTTTCTGGTTTTTTA-3′.

For transient KD, 10^6 ESCs were plated prior to transfection in gelatin-coated feeder-free 60-mm culture dishes (TrueLine) in ESC medium with LIF. The next day, the cells were transfected with 4 µg of expression vector using Lipofectamine 2000 (Invitrogen). From 1 day after transfection, the cells were selected with 2 µg/ml puromycin (Sigma-Aldrich). *C1GalT1* KD 1, *C1GalT1* KD 2, *Znrf3* KD 1, and *Znrf3* KD 2 transfected cells were cultured for 4 days post transfection. For stable *C1GalT1* KD, the appropriate constructs were transfected into ecotropic virus-packaging (PLAT-E) cells. Supernatants containing retrovirus were collected 48 h following PLAT-E transfection, mixed with 8 µg/ml polybrene (Sigma-Aldrich) and incubated with ESCs for 24 h. The following day, ESCs were replated with ESC medium containing LIF and 2 µg/ml puromycin, and selected for 7 days prior to use.

For the clonogenicity assay, 3×10^4–5×10^4 *C1GalT1* KD cells were plated on gelatin-coated 60-mm dishes in ESC medium supplemented with LIF. The cells were fixed and stained for ALP with 5-bromo-4-chloro-3-indolyl phosphate-nitroblue tetrazolium (Nacalai Tesque) 4 days after replating. The colonies were counted by microscopy and scored manually.

To analyze the effect of *O*-glycosylation inhibition, ESCs were cultured in ESC medium containing 2 mM GalNAc-Bn (Sigma-Aldrich), in the presence of LIF for 48 h.

For galectin dissociation, ESCs were cultured in ESC medium (without FBS) containing 50 mM lactose monohydrate (Kanto Chemical) for 30 min. For galectin-3 (Lgals3) addition, ESCs were cultured in ESC medium (without FBS) for 2 h before addition of 15 µg/ml Lgals3 for 30 min in ESC medium (without FBS).

Real-time PCR and RNA-seq analysis

Total RNA was extracted from cells using TRIzol reagent (Invitrogen) and reverse transcribed using a Superscript II First Strand Synthesis Kit (Invitrogen) and oligo-dT primers. Real-time PCR was performed with an ABI PRISM 7700 Sequence Detection System (Applied Biosystems) and SYBR Green Master Mix (Roche). The relative amount of each mRNA was normalized against the β-actin or *Gapdh* mRNA level in the same sample.

ST6GalNAc-I, *C1GalT1*, *β3GnT6*, and *Gapdh* copy number was calculated as previously described (Whelan et al., 2003). In brief, a region of 80–1000 bp of the *ST6GalNAc-I*, *C1GalT1*, *β3GnT6*, and *Gapdh* genes was inserted into a pGEM®-T easy vector (Promega). The vectors were linearized and a concentration ranging 100–0.01 pg/µl diluted in 1 µg/ml yeast tRNA was obtained by serial dilution to create a standard curve for each gene. The primer sets are listed in Table S1.

For RNA-seq analysis using a next-generation sequencer (NGS), a QuantSeq 3′ mRNA Seq Library Prep Kit for Illumina (FWD) (LEXOGEN, Vienna, Austria) was used to prepare libraries. RNA sequencing was performed on a NextSeq500 (Illumina, San Diego, CA, USA) in a 75-base single-end mode. The RNA-seq data were analyzed using the Strand NGS software, v3.2 (Strand Life Sciences, Bangalore, India).

Cellular *O*-glycome analysis

ESCs (~1×10^6) were homogenized using an Ultrasonic Homogenizer (Taitec Corp) as previously described (Furukawa et al., 2015a). The concentrated cellular proteins were then subjected to microwave-assisted β-elimination in the presence of a pyrazolone (BEP) reaction using a microwave reactor (Monowave 300, Anton Paar). After the reaction, 25 pmol bis-PMP-labeled N, N′, N″, N‴-tetraacetyl chitotetraose (GN4) was added as an external standard to the reaction mixture for glycan quantification. PMP-labeled *O*-glycans were purified and subjected to matrix-assisted laser desorption ionization–time of flight mass spectrometry (MALDI-TOF MS) analysis.

Tandem MALDI-TOF MS analysis

MALDI-TOF MS analysis was carried out as previously described (Furukawa et al., 2015b). Briefly, all measurements were performed using an Ultraflex II TOF/TOF mass spectrometer equipped with a reflector and controlled by the FlexControl 3.0 software package (Bruker Daltonics) in accordance with the standard protocols. All spectra were obtained in reflecton mode with an acceleration voltage of 25 kV, a reflector voltage of 26.3 kV, and a pulsed ion extraction of 160 ns in positive ion mode. Absolute quantification was performed by comparative analyses between the areas of the MS signals derived from *O*-glycans and a known amount of the internal standard bis-PMP-labeled N, N′, N″, N‴-tetraacetyl chiotetraose (GN4).

FACS analysis

A single-cell suspension was obtained using 0.02% EDTA in PBS. Subsequently, 2×10^5–3×10^5 cells were collected and washed in fluorescence-activated cell sorting (FACS) buffer [0.5% BSA (Iwai), 0.1% sodium azide (Sigma-Aldrich) in PBS]. After washing, the cell suspension was incubated with PE-conjugated anti-SSEA-1 Ab (Immunotech; 1954; 1:3), FITC-conjugated PNA (Cosmo Bio; J514; 1:100), FITC-conjugated HPA (EY Laboratories; F-3601-1; 1:100) or FITC-conjugated SNA (EY Laboratories; F-6802-1; 1:100) in FACS buffer. The cells were then analyzed using a BD FACSAria III Cell Sorter (Becton Dickinson). Cells were gated to exclude debris, dead cells (identified by propidium iodide staining; Sigma-Aldrich) and doublets.

Immunostaining

Cells were fixed with 4% paraformaldehyde in PBS (PFA/PBS) and washed in PBS. The fixed cells were blocked with 10% Block Ace (Dainihon Pharmaceutical) in PBS (Block Ace/PBS), 10% Block Ace/PBS or 1% BSA/PBS with 0.3% Triton X-100 (Sigma-Aldrich) for the analysis of cell surface or intracellular molecules, respectively. For primary labeling, the cells were incubated with PNA conjugated to biotin (PNA–biotin; Cosmo Bio; J214; 1:100), anti-Fzd5 Ab (Sigma-Aldrich; SAB4503132; 1:100), anti-β-catenin Ab (Cell Signaling; #9562; 1:100), anti-Rab5 Ab (Cell Signaling; #46449; 1:100), anti-Lgals3 Ab (Santa Cruz Biotechnology; sc-32790; 1:100) or anti-Znrf3 Ab (Bioss; bs-9141R; 1:100). Subsequently, the cells were stained with Alexa Fluor 555-conjugated streptavidin (Life Technologies; S32355; 1:300), Alexa Fluor 488-conjugated goat anti-rabbit-IgG (Life Technologies; A-11008; 1:300), Cy5-conjugated goat anti-mouse IgG (Life Technologies; A-10524; 1:300) and Hoechst 33342 (Invitrogen; H3570; 5 µg/ml). Images were obtained using an LSM 700 confocal laser microscope (Carl Zeiss). Puncta staining and the nuclear: cytoplasmic intensity ratio was quantified using Fiji (ImageJ) software. 3D reconstruction of the images was created using Imaris version 9.3.1 (https://imaris.oxinst.com).

Western and lectin blotting

Cells were lysed with lysis buffer [50 mM Tris-HCl pH 7.4, 150 mM NaCl, 1% Triton X-100, 5 mM EDTA, 1 mM Na_3VO_4, 10 mM NaF, 1 mM PMSF (Sigma-Aldrich), 2 µg/ml leupeptin (Sigma-Aldrich), 0.7 µg/ml pepstatin A (Sigma-Aldrich), 2 µg/ml aprotinin (Sigma-Aldrich), and 1 µg/ml antipain (Sigma-Aldrich)]. Protein samples were separated by SDS-PAGE and transferred to polyvinylidene fluoride membranes (Millipore). For western blotting, membranes were blocked using 1% BSA and incubated with the following primary antibodies: anti-Sox2 Ab (R&D Systems; MAB2018; 1:1000), anti-Oct3/4 Ab (Santa Cruz Biotechnology; sc-5279; 1:1000), anti-β-actin Ab (Sigma-Aldrich; A5441; 1:10,000), anti-p-β-catenin Ab (Cell Signaling; #9561; 1:1000), anti-β-catenin Ab (Cell Signaling; #9562; 1:1000), anti-Fzd5 Ab (Sigma-Aldrich; SAB4503134; 1:1000), anti-Erk1/2 Ab (Cell Signaling; #9102L; 1:1000), anti-p-Erk1/2 Ab (Cell Signaling; #9101L; 1:1000), anti-Akt Ab (BD Biosciences;

610836; 1:1000), anti-p-Akt Ab (Cell Signaling; #9275; 1:1000), anti-LRP5 Ab (Cell Signaling; #5731; 1:500), or anti-LRP6 Ab (Cell Signaling; #3395; 1:1000). The membranes were then incubated with HRP-conjugated anti-rabbit IgG (Cell Signaling; #7074; 1:10,000), anti-rabbit IgG light chain specific (Jackson Immunoresearch; 211-032-171; 1:10,000) or anti-mouse IgG (Cell Signaling; #7076; 1:10,000) secondary Abs. For lectin analysis, membranes were probed with PNA conjugated to horseradish peroxidase (HRP) (Cosmo Bio; J414; 1:10,000). The membranes were then washed, and developed with ECL Plus reagents (GE Healthcare).

Luciferase assay

A shRNA expression vector targeting *C1GalT1* (2 µg) was co-transfected using Lipofectamine 2000 with the reporter plasmid TOPFLASH (Upstate Biotechnology; 2 µg) or FOPFLASH (Upstate Biotechnology; 2 µg); pCH110 (GE Healthcare; 0.2 µg) was used as a control for transfection efficiency. Cells were lysed 4 days after transfection. Luciferase activity was measured by Dual-Light System (Applied Biosystems). Luminescence was measured with a Lumat LB9501 luminometer (Berthold).

Immunoprecipitation and pull-down assay

Cells were lysed with lysis buffer (50 mM Tris-HCl pH 7.4, 150 mM NaCl, 1% Triton X-100, 5 mM EDTA, 1 mM Na_3VO_4, 10 mM NaF, and protease inhibitors). A sample (100–500 µg) of proteins was diluted 10-fold with wash buffer [50 mM Tris-HCl pH 7.4, 150 mM NaCl, 5 mM EDTA, 1 mM Na_3VO_4, 10 mM NaF, 1 mM PMSF (Sigma-Aldrich), 2 µg/ml leupeptin (Sigma-Aldrich), 0.7 µg/ml pepstatin A (Sigma-Aldrich), 2 µg/ml aprotinin (Sigma-Aldrich), and 1 µg/ml antipain (Sigma-Aldrich)]. For immunoprecipitation, anti-Fzd5 Ab (Sigma-Aldrich; SAB4503134; 1 µg), anti-LRP5 Ab (Cell Signaling; #5731; 1 µg), anti-LRP6 Ab (Cell Signaling; #3395; 1 µg), or normal rabbit IgG (R&D Systems; AB-105-C; 1 µg) was added to the diluted cell lysate. Protein G Magnetic Beads (New England Biolabs) were then added. For the pulldown assay, the diluted cell lysate was incubated with PNA–biotin (Cosmo Bio; J214; 20 µg); streptavidin magnetic beads (Bio-Rad) were then added. The precipitated fractions were then washed five times with wash buffer. The surface biotinylation assay was performed using the Pierce cell surface protein isolation kit (Thermo Scientific) following the manufacturer's instructions.

Immunoelectron microscopy

ESCs (5×10^5) were plated on gelatin-coated 35-mm plastic dishes (TrueLine) in ESC medium with LIF. At 4 days after transfection, cells were fixed with 4% PFA and 0.01% glutaraldehyde in PBS for 1 h at room temperature and washed in PBS. The fixed cells were permeabilized with 0.5% saponin in PBS for 5 min and unreacted aldehyde functional groups were quenched using 10 mM glycine in PBS for 5 min. After PBS washing, the cells were blocked with 5% donkey serum (Jackson Immunoresearch) in PBS and incubated with anti-Fzd5 Ab against the N-terminal region (Sigma-Aldrich; SAB4503132; 1:100) or anti-Fzd5 Ab against the C-terminal region (Sigma-Aldrich; SAB4503134; 1:100) in 5% donkey serum, PBS and 0.1% Tween 20 at 4°C overnight. Subsequently, the cells were stained with ultrasmall gold-DARabbit IgG (Nanoprobes; 1:100) for 1 h at room temperature and washed with PBS. The cells were then postfixed with 1% glutaraldehyde and 0.5% tannic acid for 30 min. Following silver-enhancement of the gold particles, the cells were postfixed with 0.5% OsO_4 in 100 mM phosphate buffer (pH 7.3) for 30 min and dehydrated in a graded series of ethanol. After passage through propylene oxide, the cells were embedded in Epon 812. Ultrathin sections were cut, stained with uranyl acetate and lead citrate, and observed with a transmission electron microscope (JEM-1010C; JEOL).

Statistical analysis

An unpaired two-tailed Student's *t*-test was used to compare data with the control groups. The experiments were performed in triplicate unless stated otherwise. Statistical significance is denoted by asterisks: $*P<0.05$, $**P<0.01$, $***P<0.001$.

Acknowledgements

The authors would like to thank Prof. Yamamoto Kazuo for deep insights regarding the lectins used, Prof. Oki Shinya for ChIP atlas software training, Kazue Okada and Ikuko Yokota for the technical contributions to *O*-glycan analysis, and Ms Matsubara and Ms Hayakawa for immunoelectron microscopy technical assistance. Finally, we thank Miura Taichi and Ogura Chika for the constructive discussion and advice.

Competing interests

The authors declare no competing or financial interests.

Author contributions

Conceptualization: F.P., S.N.; Methodology: F.P., Y.A.; Validation: F.P.; Formal analysis: F.P.; Investigation: F.P., Y.A., H.H., J.-i.F., Y.I.; Resources: Y.A., H.H., J.-i.F., Y.S., Y.I., S.N.; Data curation: F.P., Y.A., H.H., J.-i.F., Y.S., Y.I.; Writing - original draft: F.P., Y.A., J.-i.F., Y.I.; Writing - review & editing: S.N.; Visualization: F.P., Y.A.; Supervision: S.N.; Project administration: S.N.; Funding acquisition: S.N.

Funding

This research was supported by Japan Society for the Promotion of Science (JSPS) KAKENHI Grant Number JP18K06139 (to S.N.) and Japan Science and Technology Agency (JST)-Mirai Program Grant Number JPMJMI18GB (to S.N.), Japan. F.P. was supported by Ministry of Education, Culture, Sports, Science and Technology of Japan (MEXT) Scholarship (Top Global University Project).

Data availability

RNA-seq data generated for this study has been deposited in the GEO repository under accession number GSE152688.

Supplementary information

Supplementary information available online at
https://jcs.biologists.org/lookup/doi/10.1242/jcs.245845.supplemental

Peer review history

The peer review history is available online at
https://jcs.biologists.org/lookup/doi/10.1242/jcs.245845.reviewer-comments.pdf

References

Bennet, E. P., Mandel, U., Clausen, H., Gerken, T. A., Fritz, T. A. and Tabak, L. A. (2012). Control of mucin-type *O*-glycosylation: a classification of the polypeptide GalNAc-transferase gene family. *Glycobiology* **22**, 736-756. doi:10.1093/glycob/cwr182

Brockhausen, I., Schachter, H., Stanley, P. (2009). O-GalNAc Glycans. In *Essentials of Glycobiology*, 2nd edn (ed. A. Varki, R. D. Cummings, J. D. Esko et al.), pp. 1-21. Cold Spring Harbor, NY: Cold Spring Harbor Laboratory Press.

Brunt, L. and Scholpp, S. (2018). The function of endocytosis in Wnt signaling. *Cell. Mol. Life Sci.* **75**, 785-795. doi:10.1007/s00018-017-2654-2

Carter, M. G., Smagghe, B. J., Stewart, A. K., Rapley, J. A., Lynch, E., Bernier, K. J., Keating, K. W., Hatziioannou, V. M., Hartman, E. J. and Bamdad, C. C. (2016). A primitive growth factor, $NME7_{AB}$ is sufficient to induce stable naïve state human pluripotency; reprogramming in this novel growth factor confers superior differentiation. *Stem Cells* **34**, 847-859. doi:10.1002/stem.2261

Dahl, J. A., Jung, I., Aanes, H., Greggains, G. D., Manaf, A., Lerdrup, M., Li, G., Kuan, S., Li, B., Lee, A. Y. et al. (2016). Broad histone H3K4me3 domains in mouse oocytes modulate maternal-to-zygotic transition. *Nature* **537**, 548-552. doi:10.1038/nature19360

Evans, M. J. and Kaufman, M. H. (1981). Establishment in culture of pluripotential cells from mouse embryos. *Nature* **292**, 154-156. doi:10.1038/292154a0

Fujitani, N., Furukawa, J.-I., Araki, K., Fujioka, T., Takegawa, Y., Piao, J., Nishioka, T., Tamura, T., Nikaido, T., Ito, M. et al. (2013). Total cellular glycomics allows characterizing cells and streamlining the discovery process for cellular biomarkers. *Proc. Natl. Acad. Sci. USA* **110**, 2105-2110. doi:10.1073/pnas.1214233110

Furukawa, J., Piao, J., Yoshida, Y., Okada, K., Yokota, I., Higashino, K., Sakairi, N. and Shinohara, Y. (2015a). Quantitative *O*-glycomics by microwave-assisted β-elimination in the presence of pyrazolone analogues. *Anal. Chem.* **87**, 7524-7528. doi:10.1021/acs.analchem.5b02155

Furukawa, J.-I., Sakai, S., Yokota, I., Okada, K., Hanamatsu, H., Kobayashi, T., Yoshida, Y., Higashino, K., Tamura, T., Igarashi, Y. et al. (2015b). Quantitative GSL-glycome analysis of human whole serum based on an EGCase digestion and glycoblotting method. *J. Lipid Res.* **56**, 2399-2407. doi:10.1194/jlr.D062083

Fuwa, T. J., Kinoshita, T., Nishida, H. and Nishihara, S. (2015). Reduction of T antigen causes loss of hematopoietic progenitors in *Drosophila* through the inhibition of filopodial extensions from the hematopoietic niche. *Dev. Biol.* **401**, 206-219. doi:10.1016/j.ydbio.2015.03.003

Gao, X., Liu, D., Fan, Y., Li, X., Xue, H., Ma, Y., Zhou, Y. and Tai, G. (2012). The two endocytic pathways mediated by the carbohydrate recognition domain and regulated by the collagen-like domain of galectin-3 in vascular endothelial cells. *PLoS ONE* **7**, e52430. doi:10.1371/journal.pone.0052430

Hao, J., Li, T.-G., Qi, X., Zhao, D.-F. and Zhao, G.-Q. (2006). WNT/beta-catenin pathway up-regulates Stat3 and converges on LIF to prevent differentiation of mouse embryonic stem cells. *Dev. Biol.* **290**, 81-91. doi:10.1016/j.ydbio.2005.11.011

Hao, H.-X., Xie, Y., Zhang, Y., Charlat, O., Oster, E., Avello, M., Lei, H., Mickanin, C., Liu, D., Ruffner, H. et al. (2012). ZNRF3 promotes Wnt receptor turnover in an R-spondin-sensitive manner. *Nature* **485**, 195-200. doi:10.1038/nature11019

He, S., Pant, D., Schiffmacher, A., Meece, A. and Keefer, C. L. (2008). Lymphoid enhancer factor 1-mediated Wnt signaling promotes the initiation of trophoblast lineage differentiation in mouse embryonic stem cells. *Stem Cells* **26**, 842-849. doi:10.1634/stemcells.2007-0356

Hiraki, M., Suzuki, Y., Alam, M., Hinohara, K., Hasegawa, M., Jin, C., Kharbanda, S. and Kufe, D. (2016). MUC1-C stabilizes MCL-1 in the oxidative stress response of triple-negative breast cancer cells to BCL-2 inhibitors. *Sci. Rep.* **6**, 26643. doi:10.1038/srep26643

Ishikawa, T., Tamai, Y., Zorn, A. M., Yoshida, H., Seldin, M. F., Nishikawa, S. and Taketo, M. M. (2001). Mouse Wnt receptor gene Fzd5 is essential for yolk sac and placental angiogenesis. *Development* **128**, 25-33.

Itoh, K., Akimoto, Y., Fuwa, T. J., Sato, C., Komatsu, A. and Nishihara, S. (2016). Mucin-type core 1 glycans regulate the localization of neuromuscular junctions and establishment of muscle cell architecture in *Drosophila*. *Dev. Biol.* **412**, 114-127. doi:10.1016/j.ydbio.2016.01.032

Itoh, K., Akimoto, Y., Kondo, S., Ichimiya, T., Aoki, K., Tiemeyer, M. and Nishihara, S. (2018). Glucuronylated core 1 glycans are required for precise localization of neuromuscular junctions and normal formation of basement membranes on *Drosophila* muscles. *Dev. Biol.* **436**, 108-124. doi:10.1016/j.ydbio.2018.02.017

Iwaki, J. and Hirabayashi, J. (2018). Carbohydrate-binding specificity of human galectins: an overview by frontal affinity chromatography. *Trends Glycosci. Glycotechnol.* **30**, SE137-SE153. doi:10.4052/tigg.1728.1SE

Johannes, L., Jacob, R. and Leffler, H. (2018). Galectins at a glance. *J. Cell Sci.*. **131**, jcs208884. doi:10.1242/jcs.208884

Karabasheva, D., Cole, N. B. and Donaldson, J. G. (2014). Roles for trafficking and *O*-linked glycosylation in the turnover of model cell surface proteins. *J. Biol. Chem.* **289**, 19477-19490. doi:10.1074/jbc.M114.564666

Kelly, K. F., Ng, D. Y., Jayakumaran, G., Wood, G. A., Koide, H. and Doble, B. W. (2011). β-catenin enhances Oct-4 activity and reinforces pluripotency through a TCF-independent mechanism. *Cell Stem Cell* **8**, 214-227. doi:10.1016/j.stem.2010.12.010

Koo, B.-K., Spit, M., Jordens, I., Low, T. Y., Stange, D. E., van de Wetering, M., van Es, J. H., Mohammed, S., Heck, A. J. R., Maurice, M. M. et al. (2012). Tumour suppressor RNF43 is a stem-cell E3 ligase that induces endocytosis of Wnt receptors. *Nature* **488**, 665-669. doi:10.1038/nature11308

Lakshminarayan, R., Wunder, C., Becken, U., Howes, M. T., Benzing, C., Arumugam, S., Sales, S., Ariotti, N., Chambon, V., Lamaze, C. et al. (2014). Galectin-3 drives glycosphingolipid-dependent biogenesis of clathrin-independent carriers. *Nat. Cell Biol.* **16**, 595-606. doi:10.1038/ncb2970

Lancaster, M. A. and Knoblich, J. A. (2014). Organogenesis in a dish: modeling development and disease using organoid technologies. *Science* **345**, 1247125. doi:10.1126/science.1247125

Lanner, F. and Rossant, J. (2010). The role of FGF/Erk signaling in pluripotent cells. *Development* **137**, 3351-3360. doi:10.1242/dev.050146

Lepur, A., Carlsson, M. C., Novak, R., Dumić, J., Nilsson, U. J. and Leffler, H. (2012). Galectin-3 endocytosis by carbohydrate independent and dependent pathways in different macrophage like cell types. *Biochim. Biophys. Acta* **1820**, 804-818. doi:10.1016/j.bbagen.2012.02.018

McCauley, H. A. and Wells, J. M. (2017). Pluripotent stem cell-derived organoids: using principles of developmental biology to grow human tissues in a dish. *Development* **144**, 958-962. doi:10.1242/dev.140731

Merlin, J., Stechly, L., de Beaucé, S., Monté, D., Leteurtre, E., van Seuningen, I., Huet, G. and Pigny, P. (2011). Galectin-3 regulates MUC1 and EGFR cellular distribution and EGFR downstream pathways in pancreatic cancer cells. *Oncogene* **30**, 2514-2525. doi:10.1038/onc.2010.631

Mouse ENCODE Consortium, **Stamatoyannopoulos, J. A., Snyder, M., Hardison, R., Ren, B., Gingeras, T., Gilbert, D. M., Groudine, M., Bender, M., Kaul, R. et al.** (2012). An encyclopedia of mouse DNA elements (Mouse ENCODE). *Genome Biol.* **13**, 418. doi:10.1186/gb-2012-13-8-418

Murry, C. E. and Keller, G. (2008). Differentiation of embryonic stem cells to clinically relevant populations: lessons from embryonic development. *Cell* **132**, 661-680. doi:10.1016/j.cell.2008.02.008

Nagy, A., Rossant, J., Nagy, R., Abramow-Newerly, W. and Roder, J. C. (1993). Derivation of completely cell culture-derived mice from early-passage embryonic stem cells. *Proc. Natl. Acad. Sci. USA* **90**, 8424-8428. doi:10.1073/pnas.90.18.8424

Nairn, A. V., Aoki, K., dela Rosa, M., Porterfield, M., Lim, J.-M., Kulik, M., Pierce, J. M., Wells, L., Dalton, S., Tiemeyer, M. et al. (2012). Regulation of glycan structures in murine embryonic stem cells: combined transcript profiling of glycan-related genes and glycan structural analysis. *J. Biol. Chem.* **287**, 37835-37856. doi:10.1074/jbc.M112.405233

Nakai-Futatsugi, Y. and Niwa, H. (2013). Transcription factor network in embryonic stem cells: heterogeneity under the stringency. *Biol. Pharm. Bull.* **36**, 166-170. doi:10.1248/bpb.b12-00958

Nishihara, S. (2018). Glycans in stem cell regulation: from *Drosophila* tissue stem cells to mammalian pluripotent stem cells. *FEBS Lett.* **592**, 3773-3790. doi:10.1002/1873-3468.13167

Niwa, H., Ogawa, K., Shimosato, D. and Adachi, K. (2009). A parallel circuit of LIF signalling pathways maintains pluripotency of mouse ES cells. *Nature* **460**, 118-122. doi:10.1038/nature08113

Nusse, R. and Clevers, H. (2017). Wnt/β-catenin signaling, disease, and emerging therapeutic modalities. *Cell* **169**, 985-999. doi:10.1016/j.cell.2017.05.016

Oki, S., Ohta, T., Shioi, G., Hatanaka, H., Ogasawara, O., Okuda, Y., Kawaji, H., Nakaki, R., Sese, J. and Meno, C. (2018). ChIP-Atlas: a data-mining suite powered by full integration of public ChIP-seq data. *EMBO Rep.* **19**, e46255.

Pai, P., Rachagani, S., Dhawan, P. and Batra, S. K. (2016). Mucins and Wnt/β-catenin signaling in gastrointestinal cancers: an unholy nexus. *Carcinogenesis* **37**, 223-232. doi:10.1093/carcin/bgw005

Pinho, S. S. and Reis, C. A. (2015). Glycosylation in cancer: mechanisms and clinical implications. *Nat. Rev. Cancer* **15**, 540-555. doi:10.1038/nrc3982

Price, F. D., Yin, H., Jones, A., van Ijcken, W., Grosveld, F. and Rudnicki, M. A. (2013). Canonical Wnt signaling induces a primitive endoderm metastable state in mouse embryonic stem cells. *Stem Cells* **31**, 752-764. doi:10.1002/stem.1321

Raghu, D., Mobley, R. J., Shendy, N. A. M., Perry, C. H. and Abell, A. N. (2019). GALNT3 maintains the epithelial state in trophoblast stem cells. *Cell Rep.* **26**, 3684-3697.e7. doi:10.1016/j.celrep.2019.02.093

Razawi, H., Kinlough, C. L., Staubach, S., Poland, P. A., Rbaibi, Y., Weisz, O. A., Hughey, R. P. and Hanisch, F.-G. (2013). Evidence for core 2 to core 1 *O*-glycan remodeling during the recycling of MUC1. *Glycobiology* **23**, 935-945. doi:10.1093/glycob/cwt030

Sasaki, N., Okishio, K., Ui-Tei, K., Saigo, K., Kinoshita-Toyoda, A., Toyoda, H., Nishimura, T., Suda, Y., Hayasaka, M., Hanaoka, K. et al. (2008). Heparan sulfate regulates self-renewal and pluripotency of embryonic stem cells. *J. Biol. Chem.* **283**, 3594-3606. doi:10.1074/jbc.M705621200

Sasaki, N., Hirano, T., Ichimiya, T., Wakao, M., Hirano, K., Kinoshita-Toyoda, A., Toyoda, H., Suda, Y. and Nishihara, S. (2009). The 3′-phosphoadenosine 5′-phosphosulfate transporters, PAPST1 and 2, contribute to the maintenance and differentiation of mouse embryonic stem cells. *PLoS ONE* **4**, e8262. doi:10.1371/journal.pone.0008262

Shahbazi, M. N. and Zernicka-Goetz, M. (2018). Deconstructing and reconstructing the mouse and human early embryo. *Nat. Cell Biol.* **20**, 878-887. doi:10.1038/s41556-018-0144-x

Smith, A. G. and Hooper, M. L. (1987). Buffalo rat liver cells produce a diffusible activity which inhibits the differentiation of murine embryonal carcinoma and embryonic stem cells. *Dev. Biol.* **121**, 1-9. doi:10.1016/0012-1606(87)90132-1

Steentoft, C., Vakhrushev, S. Y., Joshi, H. J., Kong, Y., Vester-Christensen, M. B., Schjoldager, K. T.-B. G., Lavrsen, K., Dabelsteen, S., Pedersen, N. B., Marcos-Silva, L. et al. (2013). Precision mapping of the human *O*-GalNAc glycoproteome through SimpleCell technology. *EMBO J.* **32**, 1478-1488. doi:10.1038/emboj.2013.79

Steinhart, Z. and Angers, S. (2018). Wnt signaling in development and tissue homeostasis. *Development* **145**, dev146589. doi:10.1242/dev.146589

ten Berge, D., Kurek, D., Blauwkamp, T., Koole, W., Maas, A., Eroglu, E., Siu, R. K. and Nusse, R. (2011). Embryonic stem cells require Wnt proteins to prevent differentiation to epiblast stem cells. *Nat. Cell Biol.* **13**, 1070-1075. doi:10.1038/ncb2314

Tian, E. and Ten Hagen, K. G. (2009). Recent insights into the biological roles of mucin-type *O*-glycosylation. *Glycoconj. J.* **26**, 325-334. doi:10.1007/s10719-008-9162-4

Tian, E., Hoffman, M. P. and Ten Hagen, K. G. (2012). *O*-glycosylation modulates integrin and FGF signalling by influencing the secretion of basement membrane components. *Nat. Commun.* **3**, 869. doi:10.1038/ncomms1874

Tran, D. T. and Ten Hagen, K. G. (2013). Mucin-type *O*-glycosylation during development. *J. Biol. Chem.* **288**, 6921-6929. doi:10.1074/jbc.R112.418558

Tserel, L., Kolde, R., Rebane, A., Kisand, K., Org, T., Peterson, H., Vilo, J. and Peterson, P. (2010). Genome-wide promoter analysis of histone modifications in human monocyte-derived antigen presenting cells. *BMC Genomics* **11**, 642. doi:10.1186/1471-2164-11-642

Wang, Q., Zou, Y., Nowotschin, S., Kim, S. Y., Li, Q. V., Soh, C.-L., Su, J., Zhang, C., Shu, W., Xi, Q. et al. (2017). The p53 family coordinates Wnt and Nodal inputs in mesendodermal differentiation of embryonic stem cells. *Cell Stem Cell* **20**, 70-86. doi:10.1016/j.stem.2016.10.002

Weinberger, L., Ayyash, M., Novershtern, N. and Hanna, J. H. (2016). Dynamic stem cell states: naive to primed pluripotency in rodents and humans. *Nat. Rev. Mol. Cell Biol.* **17**, 155-169. doi:10.1038/nrm.2015.28

Whelan, J. A., Russell, N. B. and Whelan, M. A. (2003). A method for the absolute quantification of cDNA using real-time PCR. *J. Immunol. Methods* **278**, 261-269. doi:10.1016/S0022-1759(03)00223-0

Woo, J. K., Choi, Y., Oh, S.-H., Jeong, J.-H., Choi, D.-H., Seo, H.-S. and Kim, C.-W. (2012). Mucin 1 enhances the tumor angiogenic response by activation of the AKT signaling pathway. *Oncogene* **31**, 2187-2198. doi:10.1038/onc.2011.410

Xia, L. and McEver, R. P. (2006). Targeted disruption of the gene encoding core 1 beta1-3-galactosyltransferase (T-synthase) causes embryonic lethality and defective angiogenesis in mice. *Methods Enzymol.* **416**, 314-331. doi:10.1016/S0076-6879(06)16021-8

Ying, Q.-L. and Smith, A. (2017). The art of capturing pluripotency: creating the right culture. *Stem Cell Rep.* **8**, 1457-1464. doi:10.1016/j.stemcr.2017.05.020

Ying, Q.-L., Nichols, J., Chambers, I. and Smith, A. (2003). BMP induction of Id proteins suppresses differentiation and sustains embryonic stem cell self-renewal in collaboration with STAT3. *Cell* **115**, 281-292. doi:10.1016/S0092-8674(03)00847-X

Ying, Q.-L., Wray, J., Nichols, J., Batlle-Morera, L., Doble, B., Woodgett, J., Cohen, P. and Smith, A. (2008). The ground state of embryonic stem cell self-renewal. *Nature* **453**, 519-523. doi:10.1038/nature06968

Zhan, T., Rindtorff, N. and Boutros, M. (2017). Wnt signaling in cancer. *Oncogene* **36**, 1461-1473. doi:10.1038/onc.2016.304

Zhang, X., Peterson, K. A., Liu, X. S., McMahon, A. P. and Ohba, S. (2013). Gene regulatory networks mediating canonical Wnt signal-directed control of pluripotency and differentiation in embryo stem cells. *Stem Cells* **31**, 2667-2679. doi:10.1002/stem.1371

Supplementary Figures

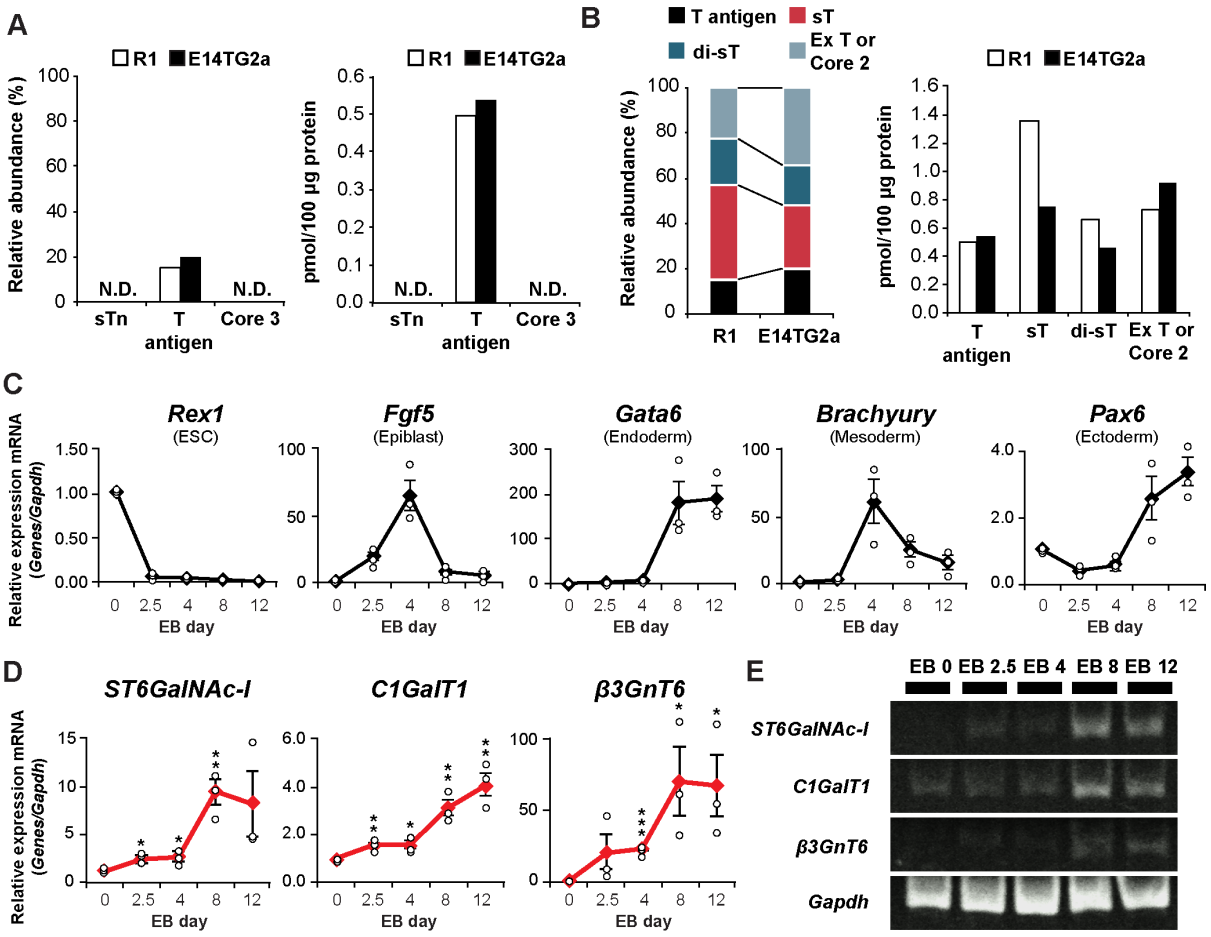

Figure S1. *C1GalT1* is the most highly expressed in ESCs and during ESCs early differentiation.

(A): Relative (left panel) and absolute amount (right panel) of sTn antigen (sTn), T antigen, and Core 3 structure (Core 3) by mass spectrometry in R1 (white box) and E14TG2a cell lines (black box). **(B):** Relative (left panel) and absolute amount (right panel) of *O*-glycan structures detected by mass spectrometry in R1 and E14TG2a cell lines. T antigen (black box), and C1GalT1-mediated elongation pathway modifications; sT antigen (sT, red box), disialyl T antigen (di-sT, dark blue box), and extended T antigen or Core 2 structure (Ex T or Core 2, light blue box). The data were obtained from a single technical and biological replicate. N.D. not detected. **(C):** Real-time PCR analysis of *Rex1, Fgf5, Gata6, Brachyury,* and *Pax6* in embryoid bodies (EB) at day 0 (ESC), 2.5, 4, 8, and 12 normalized against *Gapdh*. **(D):** Real-time PCR analysis of *ST6GalNAc-I, C1GalT1,* and *β3GnT6* in EB at day 0 (ESC),

2.5, 4, 8, and 12 normalized against *Gapdh*. **(E):** *ST6GalNAc-I, C1GalT1, β3GnT6,* and *Gapdh* mRNA quantification by PCR. mRNA was extracted from the EB at day 0 (ESC), 2.5, 4, 8, and 12 and amplified by PCR using 25 cycles to avoid saturation, and separated on polyacrylamide gel. The values are shown as means ± s.e.m. from three independent experiments**.** Significant values are indicated as * $P < 0.05$, ** $P < 0.01$, and *** $P < 0.001$.

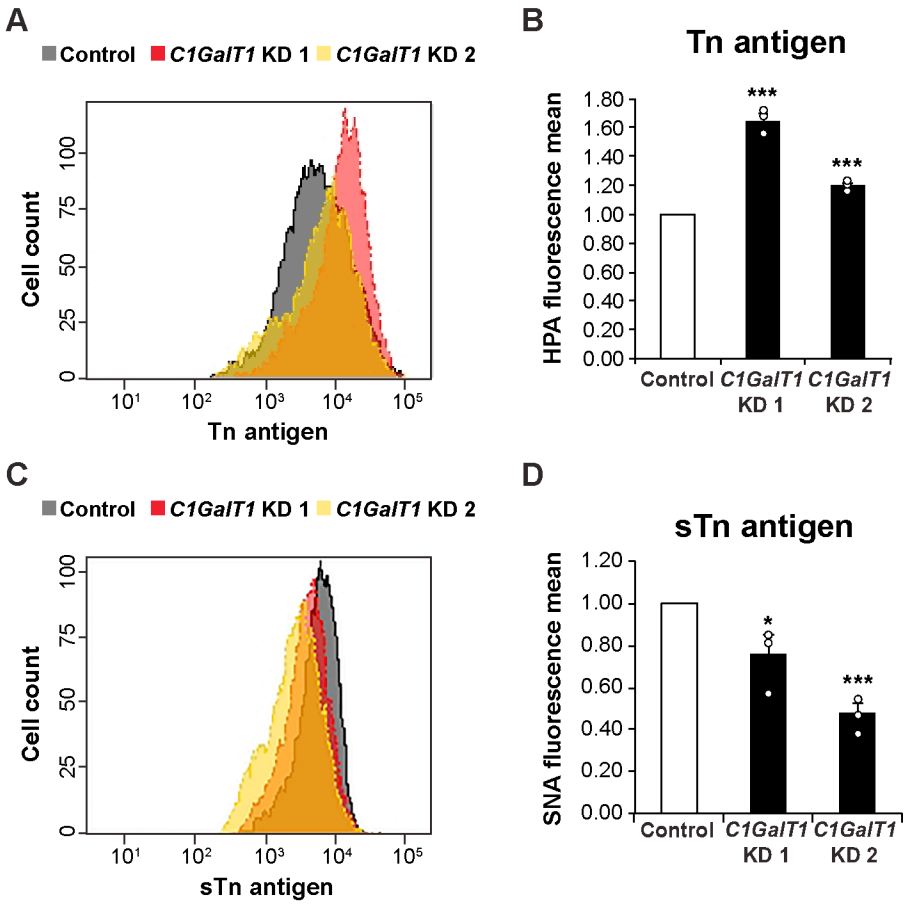

Figure S2. *C1GalT1* KD ESCs have higher levels of Tn antigen.

(A): FACS analysis in *C1GalT1* KD cells after HPA-FITC staining. **(B):** Histogram representing fluorescence mean intensity of image (**A**). **(C):** FACS analysis in *C1GalT1* KD cells after SNA-FITC staining. **(D):** Histogram representing fluorescence mean intensity of image (**C**). The fold change is relative to that of control cells. The values are shown as means ± s.e.m. of three independent experiments. Significant values are indicated as * $P < 0.05$, and *** $P < 0.001$.

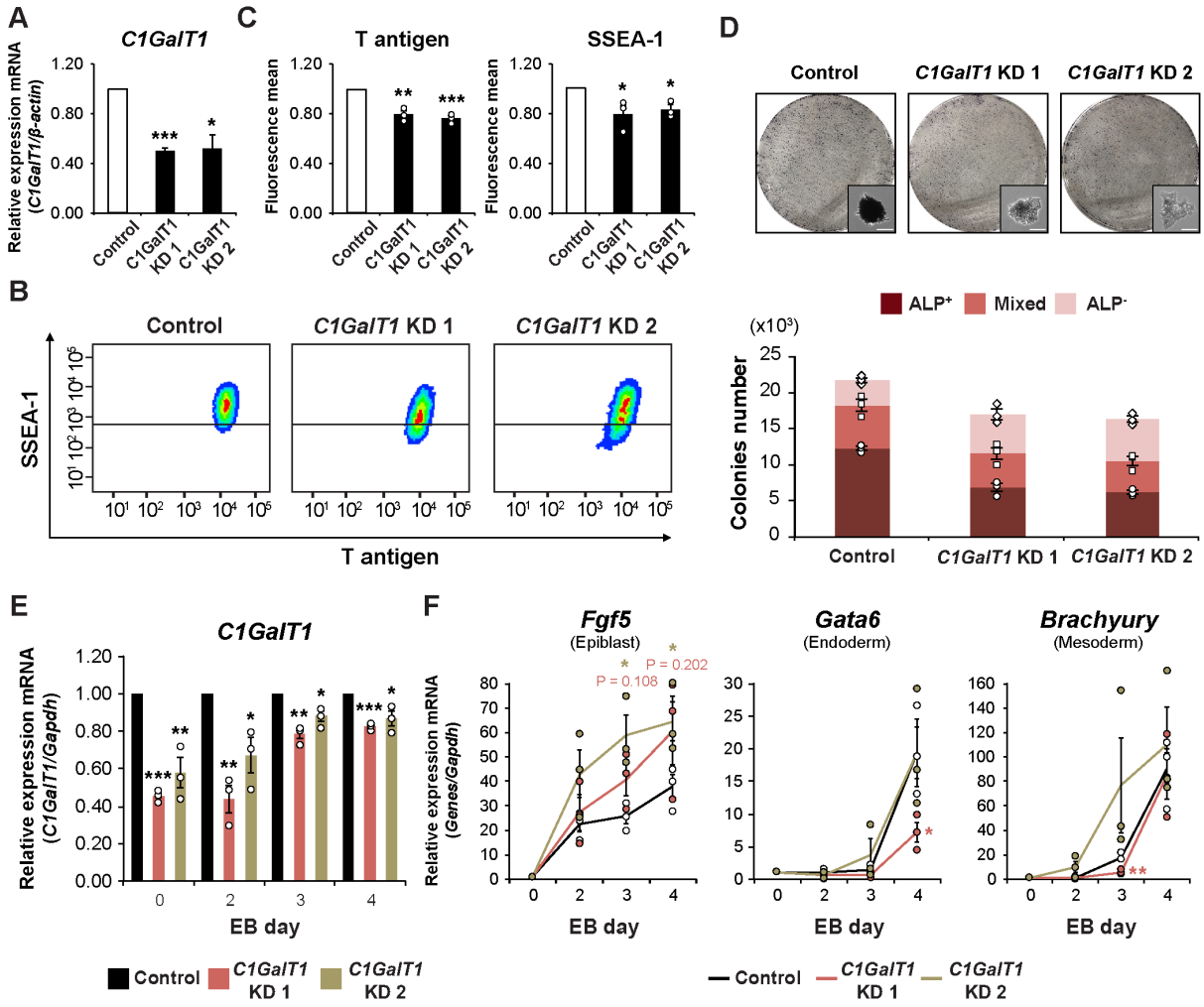

Figure S3. *C1GalT1* KD results in enhanced differentiation potential.

(A): Real-time PCR analysis of stable *C1GalT1* KD cells. The amount of *C1GalT1* was normalized against that of *β-actin*. **(B):** Density plot by FACS of stable *C1GalT1* KD cells stained with anti-SSEA-1-PE Ab and PNA-FITC. The dark line separates the SSEA-1^{+} population (upper side) and the SSEA-1^{-} population (lower side). **(C):** Histogram representing PNA-FITC and SSEA-1-PE fluorescence mean intensity of image (**B**). The fold change is relative to that of control cells. **(D):** Clonogenicity assay of stable *C1GalT1* KD cells. Scale bar, 25 µm. **(E):** Real-time PCR analysis of *C1GalT1* in embryoid bodies (EB) from transient *C1GalT1* KD ESCs plated 2 days post transfection and collected at day 0 (ESC), 2, 3, and 4 normalized against *Gapdh*. **(F):** Real-time PCR analysis of *Fgf5, Gata6,* and *Brachyury* in embryoid bodies (EB) from transient *C1GalT1* KD ESCs plated 2 days post transfection and collected at day 0 (ESC), 2, 3, and 4 normalized against *Gapdh*. The values are shown as means ± s.e.m. of three independent experiments. Significant values are indicated as * $P < 0.05$, ** $P < 0.01$, and *** $P < 0.001$.

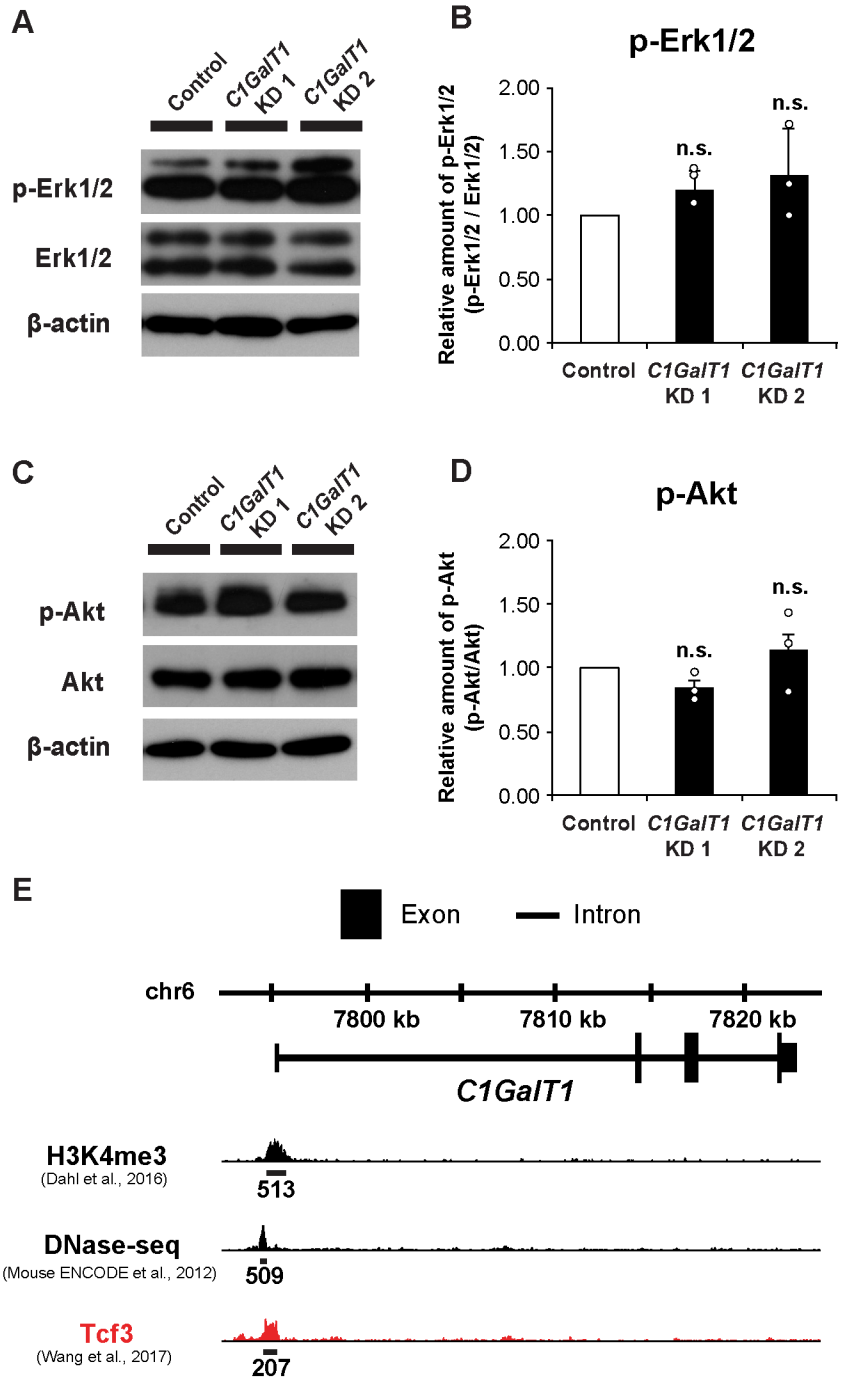

Figure S4. Knockdown of *C1GalT1* does not affect Fgf and Akt signaling. **(A):** Representative image of western blot analysis using antibodies against p-Erk1/2 and Erk1/2 in *C1GalT1* KD cells. **(B):** p-Erk1/2 western blot band intensities normalized against Erk1/2 and shown as fold change relative to control cells. **(C):** Representative image of western blot analysis using antibodies against p-Akt and Akt in *C1GalT1* KD cells. **(D):** p-Akt western blot band intensities normalized against Akt and shown as fold change relative to control cells. The values are shown as

means ± s.e.m. of three independent experiments; n.s. not significant. **(E):** ChIP-seq datasets were browsed by using ChIP-Atlas (https://chip-atlas.org). The datasets were obtained from wild-type/untreated ESCs precipitated using an anti-H3K4me3 Ab (SRX1204276) and DNase-seq (SRX191012), to identify the active promoter region and open chromatin, respectively, and by an anti-Tcf3 Ab (SRX1080398). The threshold for statistical significance was calculated by peak-caller MACS2 set as 50 ($q < 1E-05$).

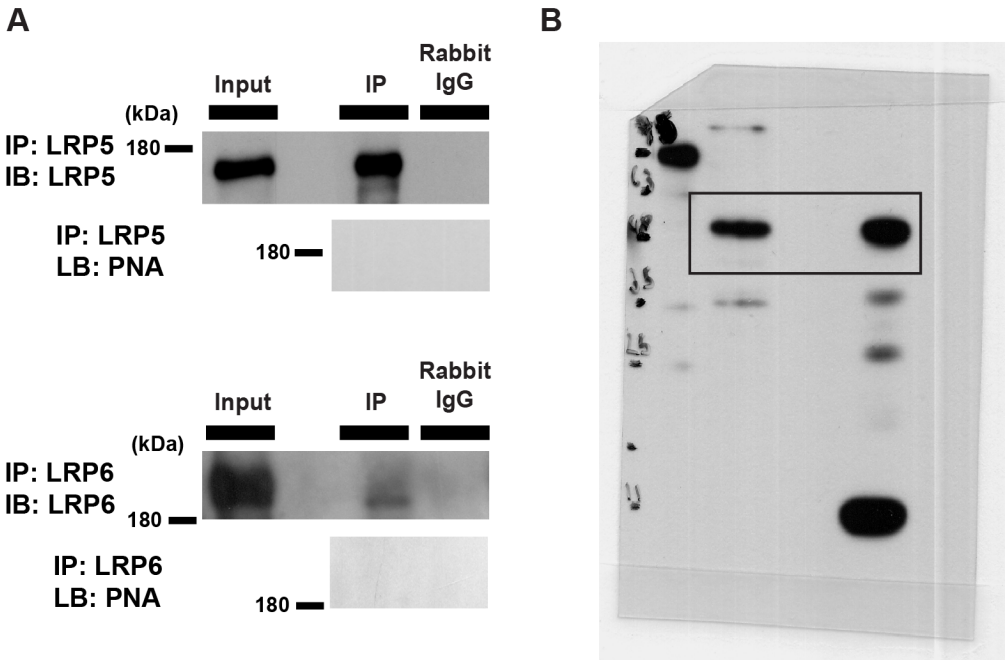

Figure S5. Frizzled co-receptors LRP5/6 do not carry T antigen.

(A): Representative images of western blot (IB) using an anti-LRP5 Ab (upper panel), or an anti-LRP6 Ab (lower panel), and lectin blot (LB) using PNA-HRP, on the immunoprecipitated fraction (IP) precipitated with an antibody against LRP5 (upper panel), or LRP6 (lower panel). The input represents the total ESC lysate. Similar results were obtained from three independent experiments. **(B):** Uncropped gel/blot relative to Fig. 5A.

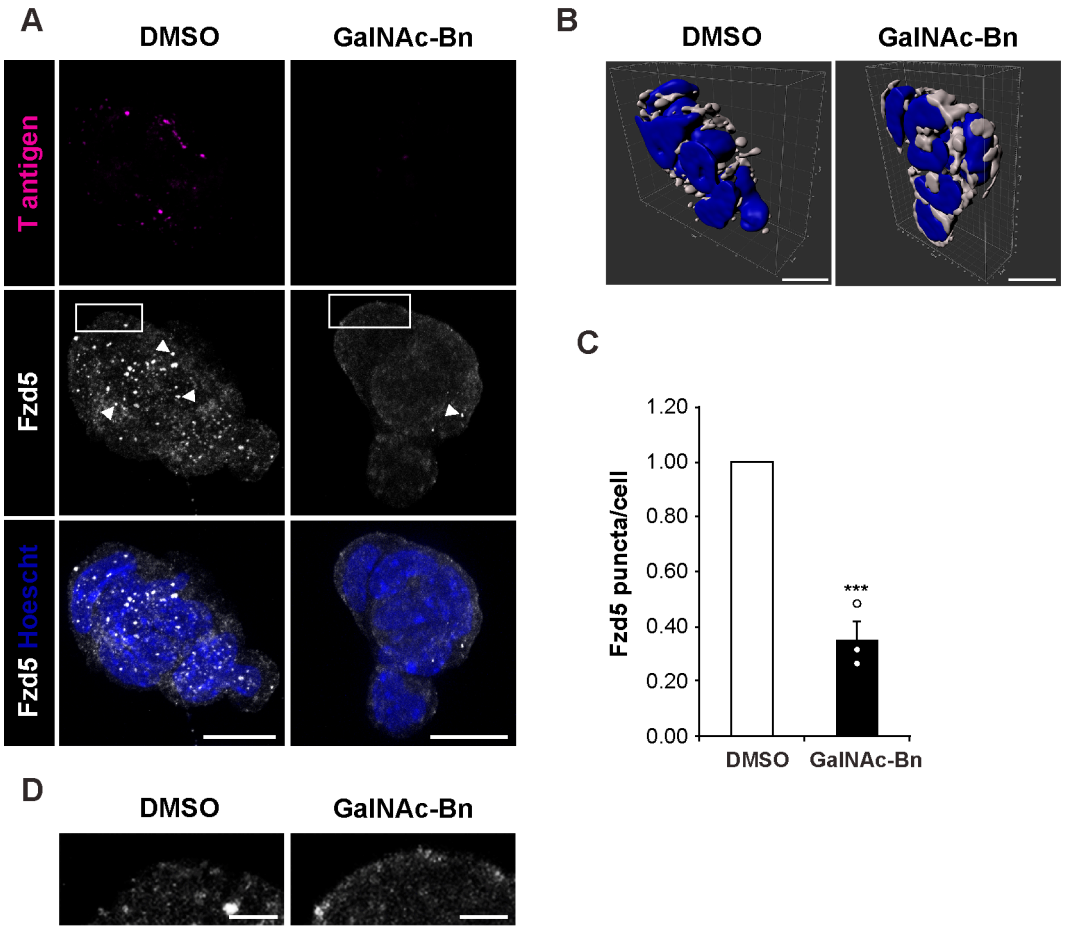

Figure S6. Mucin-type *O*-glycosylation inhibitor GalNAc-Bn reduces Frizzled-5 internalization.

(A): Representative image of a maximum intensity projection of intracellular molecules using PNA-biotin and an anti-Fzd5 Ab in the presence or absence of 2 mM GalNAc-Bn for 48 hr. Nuclei were stained with Hoechst. Arrowheads indicate Fzd5 puncta staining. Scale bar, 10 µm. **(B):** 3D reconstruction of images in **(A)** using Imaris version 9.3.1. Scale bar, 10 µm. **(C):** Quantification of Fzd5 puncta staining normalized against the number of nuclei and shown as a fold change relative to control. **(D):** Magnification of highlighted areas in image **(A)**. Scale bar, 2.5 µm. The values are shown as means ± s.e.m. of three independent experiments. Significant values are indicated as *** $P < 0.001$.

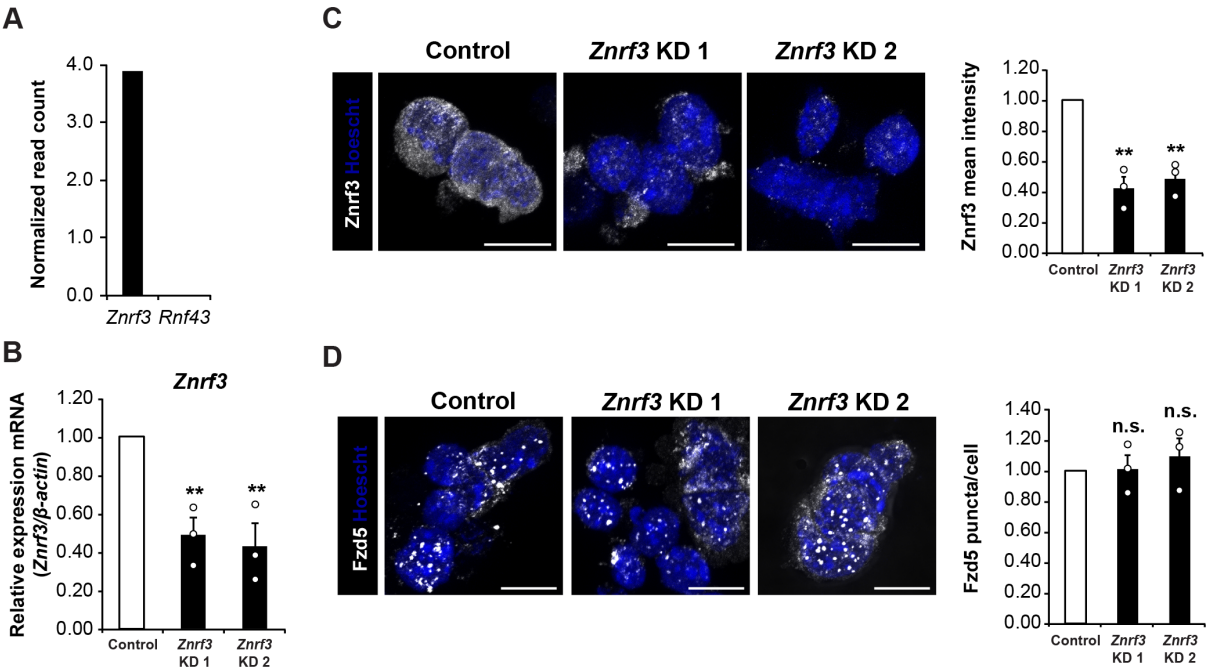

Figure S7. Znrf3 is not involved in Frizzled-5 endocytosis in ESCs.

(A): *Znrf3* and *Rnf43* expression in ESCs analyzed by RNA-seq shown as normalized read count. The data were obtained from a single technical and biological replicate. **(B):** Real-time PCR analysis of *Znrf3* KD cells. The amount of *Znrf3* was normalized against that of *β-actin*. **(C):** Representative image of a maximum intensity projection of internal molecules in *Znrf3* KD cells after immunostaining using anti-Znrf3 Ab. Nuclei were stained with Hoechst. Scale bar, 10 µm. Znrf3 mean intensity is shown as fold change relative to that of the control. (right histogram). **(D):** Representative image of a maximum intensity projection of internal molecules in *Znrf3* KD cells after immunostaining using anti-Fzd5 Ab. Nuclei were stained with Hoechst. Scale bar, 10 µm. Quantification of Fzd5 puncta staining normalized against the number of nuclei and shown as a fold change relative to control (right histogram). The values are shown as means ± s.e.m. of three independent experiments. Significant values are indicated as ** $P < 0.01$; n.s. not significant.

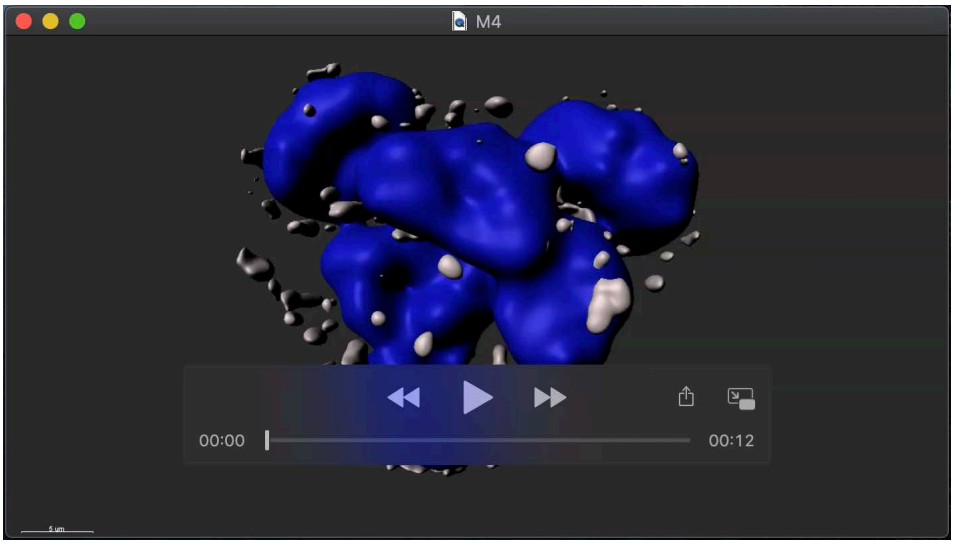

Movie 1. T antigen on Frizzled-5 regulates its endocytosis

Fzd5 puncta staining observed in control cells by 3D reconstruction. Fzd5 staining and nuclei are shown in white and blue, respectively. Scale bar 5 µm.

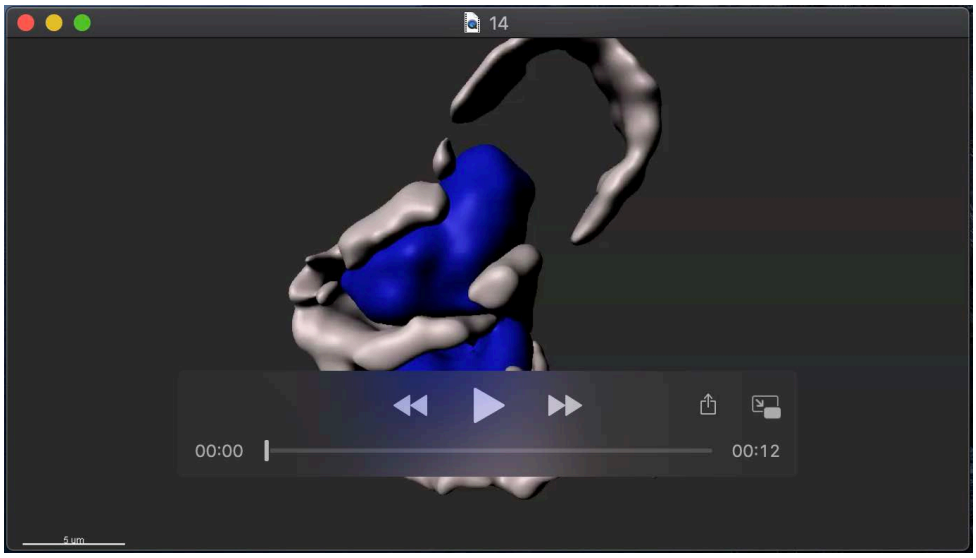

Movie 2. T antigen on Frizzled-5 regulates its endocytosis

Fzd5 membrane localization observed in *C1GalT1* KD 1 cells by 3D reconstruction. Fzd5 staining and nuclei are shown in white and blue, respectively. Scale bar 5 µm.

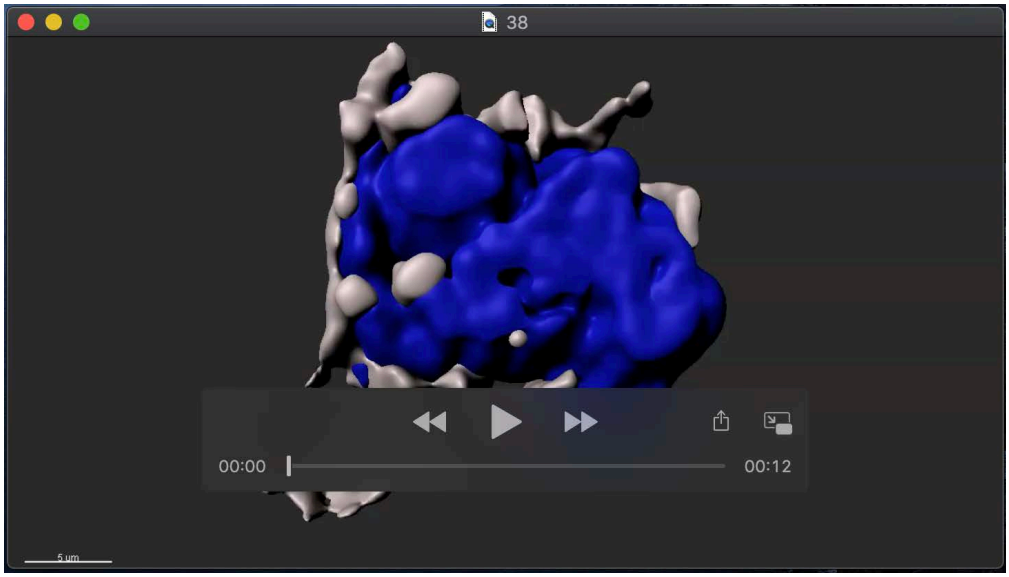

Movie 3. T antigen on Frizzled-5 regulates its endocytosis

Fzd5 membrane localization observed in *C1GalT1* KD 2 cells by 3D reconstruction. Fzd5 staining and nuclei are shown in white and blue, respectively. Scale bar 5 µm.

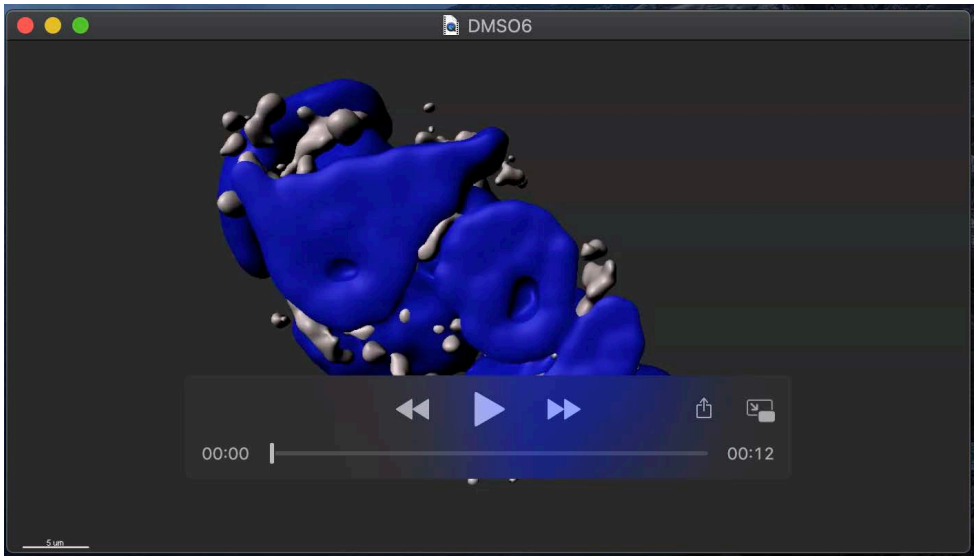

Movie 4. Mucin-type *O*-glycosylation inhibitor GalNAc-Bn reduces Frizzled-5 internalization.

Fzd5 puncta staining observed in cells treated with DMSO by 3D reconstruction. Fzd5 staining and nuclei are shown in white and blue, respectively. Scale bar 5 µm.

Movie 5. Mucin-type *O*-glycosylation inhibitor GalNAc-Bn reduces Frizzled-5 internalization.

Fzd5 membrane localization observed in cells treated with 2 mM GalNAc-Bn for 48h by 3D reconstruction. Fzd5 staining and nuclei are shown in white and blue, respectively. Scale bar 5 µm.

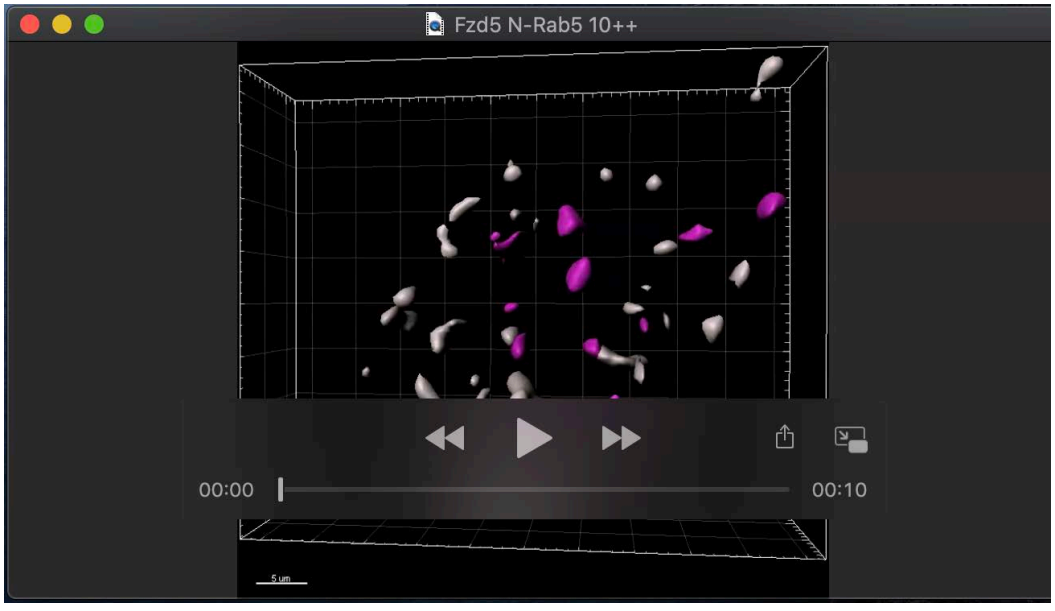

Movie 6. T antigen on Frizzled-5 regulates its endocytosis

Fzd5 and Rab5 colocalization observed in ESCs by 3D reconstruction. Fzd5 and Rab5 staining are shown in white and magenta, respectively. Scale bar at the bottom.

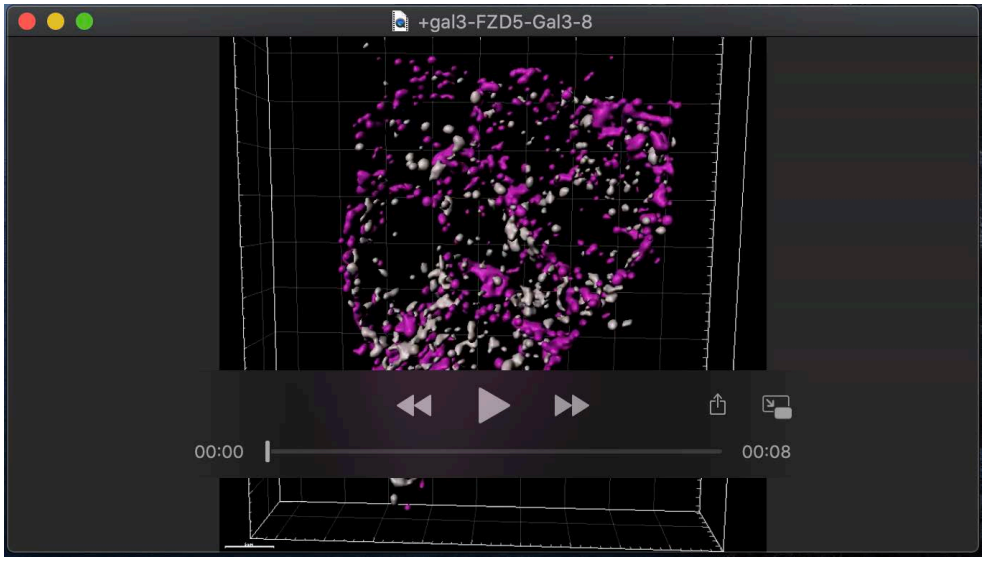

Movie 7. Frizzled-5 endocytosis is mediated by galectin-3

Fzd5 and Lgals3 colocalization observed in ESCs treated with 15 µg/mL Lgals3 for 30 minutes by 3D reconstruction. Fzd5 and Lgals3 staining are shown in white and magenta, respectively. Scale bar at the bottom.

Supplementary Table

Table S1 Primer sets

Gene	Forward primer	Reverse primer
C1GalT1	5'- GCAAGGCATTCAGATGACAA -3'	5'- ATGTTGGCTGGAATCTGCAT -3'
ST6GalNAc-I	5'- GAGAGGCAGTCCAAGGAGAGC -3'	5'- TGAGGATTCTCTGGTGCTGGC -3'
β3GnT6	5'- AGTCCCACGACACTGGCTTTC -3'	5'- CCTGCCTGTGTTCCTGGAGG -3'
Oct3/4	5'- CTCACCCTGGGCGTTCTCT -3'	5'- AGGCCTCGAAGCGACAGA -3'
Sox2	5'- ACCAGAAGAACAGCCCGGA -3'	5'- CCCGGGACCATACCATGA -3'
β-catenin	5'- GTTAAACTCCTGCACCCACCA -3'	5'- AAAGGGCAAGGTTTCGAATCA -3'
Axin2	5'- GGGAGCAGTTTTGTGGCAGCA -3'	5'- AGGGTCCTGGGTAAATGGGTGAG -3'
Fgf5	5'- GCAGCCCACGGGTCAA -3'	5'- CGGTTGCTCGGACTGCTT -3'
Otx2	5'- CATGATGTCTTATCTAAAGCAACCG -3'	5'- GTCGAGCTGTGCCCTAGTA-3'
Cdx2	5'- GAGCTGGCTGCCACACTTG -3'	5'- GCTTCTTCTTGATTTTCCTCTCCTT -3'
Gata3	5'- CCATTACCACCTATCCGCCC -3'	5'- TCGACTTACATCCGAACCCG -3'
Gata4	5'- TCCATGTCCCAGACATTCAGACT -3'	5'- AGCAGACAGCACTGGATGGAT -3'
Gata6	5'- CCCCTCATCAAGCCACAGAA -3'	5'- GTGACAGTTGGCACAGGACAGT -3'
Brachyury	5'- TGCTGCAGTCCCATGATAACTG -3'	5'- ATGACTCACAGGCAGCATGCT -3'
Mixl1	5'- GCACGTCGTTCAGCTCGGAGCAGC -3'	5'- AGTCATGCTGGGATCCGGAACGTGG -3'
FoxA2	5'- AGCCGTGAAGATGGAAGGG -3'	5'- CTCCGCGTAGTAGCTGCTCC -3'
Sox17	5'- GCACAACGCAGAGCTAAGCA -3'	5'- CTGCCAAGGTCAACGCCT -3'

Pax6	5'- AACCTGGCTAGCGAAAAGCA -3'	5'- CCCGTTCAACATCCTTAGTTTATCA-3'
Nestin	5'- TGCAGACACCTGGAAGAAGTTC -3'	5'- CCCAAGGAAATGCAGCTTCA -3'
Rex1	5'- GCTCCTGCACACAGAAGAAA -3'	5'- GTCTTAGCTGCTTCCTTCTTGA -3'
Znrf3	5'- CGGCGACTATACCACCCAC -3'	5'- GGGGTCCAATTCTGGCTGTT -3'
Gapdh (qPCR/T-vector)	5'- TGCACCACCAACTGCTTAGC -3'	5'- GGCATGGACTGTGGTCATGAG -3'
β-actin	5'- GCTCTGGCTCCTAGCACCAT -3'	5'- GCCACCGATCCACACAGAGT -3'
C1GalT1 (T-vector)	5'- CGAGAAGAGGCTGCCATTC -3'	5'- AGCATCCAGGACCCTCTAT -3'
ST6GalNAc-I (T-vector)	5'- AAGGCTGAGCCCCAAGTAC -3'	5'- GCAGTGAAGCCATAGAAGGA -3'
β3GnT6 (T-vector)	5'- AGCAGCCGCAGGTTCAAG -3'	5'- GTCGATGGGGAAGAGCGG -3'